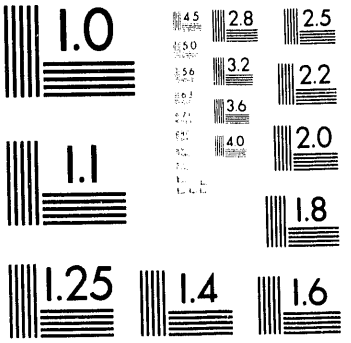
1.0
1.1
1.25
1.4
1.6
1.8
2.0
2.2
2.5
2.8
3.2
3.6
4.0
4.5
5.0
5.6

1 of 2

DOE/MC/26365-3423
(DE93000290)
Distribution Category UC-109

Hydrogen Separation by Ceramic Membranes in Coal Gasification

Final Report

G.R. Gavalas

Work Performed Under Contract No.: DE-AC21-90MC26365

For
U.S. Department of Energy
Office of Fossil Energy
Morgantown Energy Technology Center
P.O. Box 880
Morgantown, West Virginia 26507-0880

By
California Institute of Technology
Pasadena, California 91125

TABLE OF CONTENTS

Summary

The general objective of this project was to develop hydrogen permselective membranes for hydrogen production from coal gas. The project consisted of the following tasks: (i) membrane preparation and characterization, (ii) membrane stability testing, and (iii) analysis and economic evaluation of a membrane-assisted ammonia from coal process.

1. Membrane Preparation and Characterization

Several oxides (SiO_2, TiO_2, Al_2O_3, B_2O_3) in dense (or nonporous) form were identified to be permselective to hydrogen at elevated temperatures. To obtain reasonable permeance it is necessary that the membrane consists of a thin selective layer of the dense oxide supported on or within the pores of a porous support tube (or plate). Early in the project we chose porous Vycor tubes (5mm ID, 7 mm OD, 40 Å mean pore diameter) supplied by Corning Inc. as the membrane support. To form the permselective layer (SiO_2, TiO_2, Al_2O_3, B_2O_3) we employed chemical vapor deposition using the reaction of the chloride ($SiCl_4$, etc.) vapor and water vapor at high temperatures.

Deposition of the selective layer was carried out in a simple concentric tube reactor comprising the porous support tube surrounded by a wider concentric quartz tube and placed in an electrically heated split tube furnace. In one deposition geometry (the opposing reactants or two-sided geometry) the chloride vapor in nitrogen carrier was passed through the inner tube while the water vapor also in nitrogen carrier was passed in the same direction through the annulus between the two tubes. In the other (two-sided) geometry the chloride-containing stream and the water-containing stream were both passed through the inner tube or both through the annulus.

During deposition the flow of reactants was interrupted every few minutes to measure, *in situ*, the membrane permeance to hydrogen, nitrogen and occasionally other

gases. Once the permeance to nitrogen decreased by a factor of at least 100, deposition was terminated and the membrane stored for stability testing or microscopy.

Deposition of SiO_2 membranes were carried out initially in the opposing reactants geometry. The temperature was 700-800°C, the pressure atmospheric and the composition of the two reactant streams was 30% $SiCl_4$-N_2 and 7% H_2O-N_2, respectively. The membrane permeance to hydrogen at 450°C was as high as 0.1 cm^3/cm^2-min-atm and the H_2:N_2 permeance ratio was in the range 1000-5000.

Deposition of SiO_2 membranes in the one-sided geometry was much faster and produced considerably higher hydrogen permeance, as high as 0.35 cm^3/cm^2-min-atm, but lower H_2:N_2 permeance ratio (200-1000).

Titanium oxide and aluminum oxide membranes could only be produced in the opposing reactants geometry. The TiO_2 membranes had slightly lower hydrogen permeance and much lower selectivity than the SiO_2 membranes prepared in the opposing reactant geometry. The Al_2O_3 membranes also had lower permeance and selectivity than the SiO_2 membranes.

Boron oxide membranes were prepared in both the opposing and one-sided geometries. Deposition could take place at temperatures as low as 100°C and the membrane permeance at temperatures up to 450°C was as high as 0.2 cm^3/cm^2-min-atm. However, upon heating above 500°C, the membrane permeance decreased sharply. Moreover, when these membranes were exposed to humid laboratory air for extended periods, they developed microcracks and lost their selectivity.

In view of the superior properties of the silica membranes, after the initial experiments work continued only with these membranes. The purpose of the later deposition studies was to explore means of increasing membrane permeance. To this end deposition was carried out with support tubes of smaller pore diameter (25 Å) and thinner wall (0.35 mm) and with two other silicon precursors, hexachloro-disiloxane, and

octachloro-trisiloxane. Membranes with hydrogen permeance as high as 0.52 cm^3/cm^2-min-atm at 450°C were prepared with these support tubes and silica precursors.

In addition to measuring membrane permeance to different gases, membrane characterization was carried out by scanning electron microscopy (SEM) and electron microprobe analysis (EMA). SEM and EMA of SiO_2, TiO_2, Al_2O_3 membranes prepared by opposing reactants deposition revealed an asymmetric deposit layer consisting of a slowly rising section from the side of the chloride flow leading to a region of maximum density followed by a steep decline. By contrast, the density profile of the membranes prepared by one-sided deposition had their maximum at the boundary (the inner cylindrical surface) and was monotonically declining. In both types of membranes, the selectivity is due to the region around the peak of the deposit layer where Knudsen diffusion is completely interrupted and transport takes place by activated diffusion through the oxide network. The thickness of this region could not be measured accurately but was in the range 0.1-1 μm. The remaining and much thicker part of the deposit layer (10-50 μm) which involves partially plugged pores has an adverse effect on permeance without contributing much to selectivity.

2. Membrane Stability Testing

The silica membranes prepared as described above were subjected to a variety of thermal and hydrothermal treatments to test their stability under conditions pertinent to catalytic water gas shift reaction of coal gas. Immediately after preparation the membranes were annealed in dry nitrogen at 700-750°C for about 12 hours. For membranes produced in the one-sided geometry this dry annealing resulted in a slight decline of hydrogen permeance (less than 10%) and a significant decline of nitrogen permeance (by a factor 2-5) such that the H_2:N_2 selectivity improved.

One group of membranes were subjected to heating at 500-600°C in a pressure vessel containing 22% H_2, 27% CO, 32% H_2O, 18% CO_2, 1% H_2S at 10-12 atmospheres

total pressure. After four days such hydrothermal treatment, all membranes prepared in the opposing reactants geometry failed (c: :ed). The membranes prepared in the one-sided geometry did not fail but underwent s:. .ificant decline in their hydrogen permeance from about 0.2 to about 0.05 cm^3/cm^2-min-atm.

A second group of membranes of somewhat higher initial permeance, all prepared with one-sided deposition, were treated hydrothermally at 550°C for 21 days in a gas containing 32% H_2O-N_2 at 10 atmospheres total pressure. Initially the hydrogen permeance declined rapidly after which it declined slowly stabilizing to a value about three to four times below its initial value.

A third group of membranes prepared in the one-sided geometry but with different substrate tubes and silica precursors (see previous subsection) were treated hydrothermally under the same conditions as the second group for 13 days. These membranes also underwent a decline of hydrogen permeance by about a factor of four and a decline of the nitrogen permeance by a somewhat larger factor.

3. Process Analysis and Economic Evaluation

Kinetics Technology International (KTI), San Dimas, California Office, carried out analysis and economic evaluation of a membrane-assisted and a conventional process of ammonia from coal. This process was chosen as an important potential use of hydrogen from coal gasification, in order to evaluate the commercial potential of the silica membranes. The analysis and evaluation was based on the membrane properties measured at Caltech, a shift reactor model developed at Caltech, and cost estimates of Vycor tubing provided by Corning Inc.

In comparing the membrane-assisted and the conventional process, only the hydrogen production section (water gas shift unit and separation unit) was different for the two · ocesses and had to be considered. The coal gasifier and hot gas cleanup, the ammonia production unit, and the power generation unit were the same in both processes.

For the purpose of this study the coal gas was assumed to have composition typical of an oxygen-blown KRW gasifier converting about 1000 ton per day low sulfur (0.4%) coal. Both the membrane and the conventional process use the same amount and composition of coal gas and produce purified hydrogen equivalent to 560 ton per day ammonia. Both processes produce electric power as well as ammonia by using part of the coal gas in a gas turbine-steam turbine dual cycle. Much of the power generated is used for the internal needs of the process, most of it for driving the ammonia compressors and the combustion air compressors. However, there is some net power produced by both processes. Although the two processes receive the same amount of coal gas and produce the same amount of ammonia they differ in net power production and in capital cost because they employ different unit operations and equipment.

The conventional process adds a large amount of steam to the coal gas such that after two successive catalytic shift stages (high temperature and low temperature) the conversion of CO is 99+%. Pure hydrogen with only traces of CO, CO_2, CH_4 and H_2S is produced by pressure swing adsorption (PSA) and conducted to the ammonia plant. The net power production in this process was estimated to be 36.6 MW.

The membrane-assisted process requires much less steam to achieve high conversion for the shift reaction. The membrane reactor used in this process consists of three high temperature shift reactor units, each followed by a membrane unit and a heat exchanger. The permeate gas is high purity hydrogen which after methanation (to convert the few tens of a percent of CO and CO_2 to methane) is used in the ammonia plant. The nonpermeate gas containing significant fractions of hydrogen, carbon dioxide and methane (deriving from the coal gas) is fed directly to the combined cycle power generation. The net power production in the membrane-assisted process was estimated to be 44.4 MW.

To obtain a cost estimate for the membrane it was assumed that each of the three membrane units consists of series-parallel combination of several thousand membrane modules. Each membrane module in turn consists of several thousand membrane

capillaries sealed in parallel to an endplate and enclosed in a metal casing. The capillaries were assumed to have 0.5 mm ID, 0.7 mm OD and hydrogen permeance at 500°C of 0.1 cm^3/cm^2-min-atm in accordance with the values measured after hydrothermal treatment.

On the basis of the above parameters, the membrane area required by the process was calculated to be 150,000 m^2, or 19.3 tons of capillaries. The cost of the membrane units is difficult to estimate because Vycor tubes below 5 mm ID are not produced commercially. However, some very crude estimates made by Corning Inc. placed the cost at 300-600 dollars per pound. Using the figure of $500/lb and including some additional cost for the CVD treatment and the fabrication of modules and larger units, yielded a cost of about $24 million for the membrane units. Compared to this membrane cost, the conventional process requires only $6 million for the PSA unit. All other equipment are the same for both processes. Thus, the membrane-assisted process has 24 – 6 = $18 million extra cost while producing 7.8 MW extra power. With the price of power between 2 ct and 5 ct per kWhr, the extra power would generate $1.36 million to $3.4 million annually. With these figures the extra cost for the membrane would require 5 to 13 years to be recovered.

The membrane process would become competitive if the hydrogen permeance could be increased by a factor of 3 to 0.3 cm^3/cm^2-min-atm so that the extra membrane cost would be reduced to 8 – 6 = $2 million and the recovery period to 0.6-1.5 years. All these estimates are subject to considerable uncertainty due to the lack of reliable costs for the individual membrane capillaries and the fabrication of membrane modules. Further work is clearly indicated on increasing membrane permeance, developing techniques for making multi-tube modules, and generating reliable cost estimates for tubes and modules.

Introduction

Coal gasification is a promising alternative to steam reforming of natural gas as a source of hydrogen for the synthesis of ammonia and other chemicals. The hydrogen consumed in coal conversion to liquid fuels could also be derived from the gasification of coal or coal residues. In either of these uses of coal the separation of hydrogen from coal gas can be carried out by established processes like acid gas removal followed by pressure swing adsorption. However, membrane separation is a promising alternative having the potential of higher energy efficiency and simpler process flowsheet. To realize these potential advantages the separation must be carried out at elevated temperatures necessitating the use of inorganic membranes. Separation of hydrogen sufficiently pure for ammonia or other chemical synthesis requires membranes of very high selectivity, while separation of less pure hydrogen for use in coal liquefaction is feasible with less selective membranes. In the case of hydrogen production for chemical synthesis the use of hydrogen permselective inorganic membranes permits the integration of hydrogen separation and catalytic shift reaction in a membrane reactor in order to simplify the flowsheet and improve the economics of the process.

Both mesoporous (2-50 nm diameter) and nonporous inorganic membranes have been investigated from the standpoint of gas separations. Japanese investigators[1-4] have studied the separation of gases by porous glass membranes with pore of size 30-50 Å. Membranes with similar pore size were made by sol gel techniques depositing a coating of mesoporous γ-Al_2O_3 on macroporous α-Al_2O_3 and are available commercially as filters for liquids purification.[5-10] Reference[4] describes the application of mesoporous (30-50 Å) silica glass membranes and γ-Al_2O_3 membranes to the catalytic dissociation of H_2S with simultaneous H_2 separation.

Governed by Knudsen diffusion, the separation selectivities of microporous membranes are generally too low for membrane-reactor applications. For example, the ratio of Knudsen diffusivities for the H_2:CO pair is only 3.74. Only activated diffusion through nonporous or molecular sieve materials can provide higher selectivities. Palladium and its alloys are known to be highly and selectively permeable to hydrogen and have been studied in connection with certain dehydrogenation reactions. The high cost of palladium and its sensitivity to poisoning by sulfur are obstacles to its applications to coal gas processing. Certain base metals (V, e.g.) are also semipermeable to hydrogen. Currently metal membranes are being developed under DOE funding for application to the water gas shift reaction and the conversion of hydrogen sulfide to elemental sulfur.[11] These composite membranes consist of a vanadium sheet surrounded at both sides by a SiO_2 interdiffusion layer and an outer layer of a noble metal (e.g. Pt). The role of the noble metal is to catalyze the dissociation of molecular hydrogen to atomic hydrogen as required for dissolution and transport through the V layer. Considerations of membrane stability and cost will ultimately determine the economic viability of these membranes.

Besides metals, silica glass is known to be highly selective for hydrogen permeation.[12] For example, at 500°C the permeability of hydrogen through Vycor glass is more than four orders of magnitude higher than that of O_2. This selectivity towards hydrogen is due to the relatively easy permeation of the small hydrogen molecule through the glass network with other gases (O_2, N_2, CO, etc.) permeating extremely slowly. That low permeation rate makes SiO_2 unsuitable for separations other than those involving hydrogen. The permeation rate depends on the composition of the glass and increases rapidly with temperature. To the best of our knowledge nonporous silica glass has not been studied before as a material for gas separations although, in addition to its high selectivity, it is easy to fabricate in a membrane configuration. The practical application of SiO_2 membranes requires that they possess adequate permeation rates as well as good selectivity. These two requirements can be met by preparing the membrane in composite

form, consisting of a thin layer of the dense oxide (silica, etc.) supported on a porous tube or plate--tube being the more practical geometry.

Deposition of silica and other oxide layers on porous support tubes or plates can be carried out by liquid phase or gas phase techniques. The oxide layers deposited by liquid phase techniques are porous, for driving off a solvent or a reaction product during drying and calcination leaves behind a porous structure. Gas phase techniques--chemical vapor deposition (CVD)--can, in principle, produce a dense (nonporous) deposit layer because the reaction products are removed during deposition and no drying or calcination steps are necessary.

Dense silica membranes were first prepared at Caltech using the oxidation of silane (SiH_4). The reaction was carried out in the opposing reactants geometry, i.e. passing one reactant (SiH_4) through the bore of the porous Vycor tube, and the other (O_2) past the outside surface of the tube; both at atmospheric pressure. The reactants diffuse and react within a certain region within the porous matrix. Once the open pore paths are interrupted, the reaction essentially ceases and the resulting nonporous layer provides the desired membrane function. The results of this work utilizing SiH_4 oxidation have been reported earlier.[13-15]

Silica deposition by SiH_4 oxidation is limited to a relatively narrow temperature window, 400-500°C. Below 400°C the reaction is too slow producing a thick layer, therefore low membrane permeance. Above 500°C silane pyrolysis becomes significant producing elemental silicon over a wide region of the porous support, therefore again resulting in very low permeance. When the silica membranes produced by SiH_4 oxidation was heated at temperatures above 450°C in the presence of water vapor they suffered a sharp decline of permeance and often a decline of selectivity as well. When water vapor was added to the SiH_4 and O_2 reactants during CVD, subsequent exposure to high temperature and water vapor caused loss of hydrogen permeance but improved the selectivity somewhat.

Chemical vapor deposition of silica can be carried out by hydrolysis of silicon tetrachloride ($SiCl_4$) as well as by oxidation of SiH_4. Silicon tetrachloride does not decompose thermally like SiH_4, therefore the hydrolysis can be carried out at temperatures as high as 800°C, above which, however, the porous structure of the Vycor support may start collapsing. Increasing the reaction temperature can, in principle, produce thinner deposit layers and, hence, higher membrane permeance. Besides its higher thermal stability, silicon tetrachloride is not flammable, unlike SiH_4, and hence safer to handle. It is also quite inexpensive being an intermediate in the production of silicon and silicones. However, it is corrosive in the presence of humidity.

In addition to $SiCl_4$, certain other volatile chlorides can be hydrolyzed in the gas phase to the respective oxides. These include $TiCl_4$, $AlCl_3$, and BCl_3. Boron oxide (B_2O_3) is amorphous and is known to be hydrogen permselective and have higher hydrogen permeability than SiO_2. The other two oxides TiO_2 and Al_2O_3 had not been investigated as hydrogen permselective materials.

This project was initiated with the objective to (i) prepare membranes of SiO_2, TiO_2, Al_2O_3 and B_2O_3 supported on porous Vycor tubes by the hydrolysis of the respective chlorides, (ii) characterize the morphology and permeation properties of these membranes, (iii) test the membrane stability in contact with coal gas under conditions typical of the water gas shift reaction, (iv) develop a membrane reactor model for the water gas shift reaction and (v) conduct an economic analysis of membrane application to hydrogen production from coal gas.

This report is organized in four chapters. Chapter 1 describes the work on membrane preparation and characterization. Chapter 2 describes the stability testing. Chapter 3 is the process analysis and evaluation carried out by KTI, but also includes an appendix on membrane reactor modeling. The final Chapter 4 contains the general conclusions.

Literature Cited

1. Kameyama, T., Dokiya, M., Yokokawa, H. and Fukuda, K. *Ind. Engng. Chem. Fundam.* **20**, 97 (1981).
2. Shindo, Y., Hakuta, T., Yoshitome, H. and Inoue, H., *Chem. Engng. Japan* **17**, 650 (1984).
3. Shindo, Y., Hakuta, T., Yoshitome, H. and Inoue, H., *J. Chem. Engng. Japan* **18**, 485 (1985).
4. Haraya, K., Shindo, Y., Hakuda, T and Yoshitome, H., *J. Chem. Engng. Japan* **19**, 186 (1986).
5. Leenaars, A. F. M. and Burggraaf, A. J., *J. Colloid Interface Sci.* **105**, 27 (1978).
6. Keizer, K., Leenaars, A. F. M. and Burggraaf, A. J., in *The Science of Ceramics*, Vol. 12, Ceramurgica, Faenza, 1984.
7. Chu, P.-Y. and Clark, D. E., *Advanced Ceramic Materials* **3**, 249 (1988).
8. Okubo, T., Watanabe, M., Kusakabe, K. and Morrooka, S., *J. Materials Sci.* **25**, 4822 (1990).
9. Okubo, T., Haruta, K., Kusakabe, K. and Morooka, S., *J. Membrane Sci.* **59**, 73 (1991).
10. Cini, P., Blaha, S. R., Harold, M. P. and Venkataraman, K., *J. Membrane Sci.* **55**, 199 (1991).
11. Edlund, D. J., abstract of a paper presented at the 12th annual gasification and gas stream cleanup systems contractors review meeting, Morgantown Energy Technology Center, September 15-17, 1992.
12. Boyd, D. C. and Thompson, D. A., "Glass" *Encyclopedia of Chemical Technology* **11**, 807 (1980).
13. Gavalas, G. R., Megiris, C. E. and Nam, S. W., *Chem. Eng. Sci.* **44** 1829 (1989).
14. Nam, S. W. and Gavalas, G. R., *AIChE Symp. Ser.* **85**, 68 (1989).
15. Gavalas, G. R. and Megiris, C. E., U.S. Patent 4,902,307, 1990.

Chapter 1

Membrane Preparation and Characterization

1.1 Introduction

This chapter describing the membrane preparation and characterization work constitutes the major part of this project. Several variations of membrane layer deposition were tested in the effort to improve the hydrogen permeance without undue compromise in selectivity. One variation was in the material of the selective layer. Titanium, aluminum and boron oxides were tested in addition to silicon oxide. Another variation was in the geometry of deposition--one sided versus opposing reactants geometry. A third was in the gas phase reagent and a final variation was in the wall thickness and porous structure of the support tube. Silica turned out to be superior to the other three oxides, hence, the latter phases of the project were devoted exclusively to silica membranes.

The variations of deposition geometry, gaseous silica precursors, and support tubes were examined with the purpose of increasing the rate of the deposition reaction relative to that of diffusion (increasing Thiele modulus) thereby reducing the thickness of the deposit layer and increasing the hydrogen permeance. Of these variations decreasing the pore size of the support turned out to be the most beneficial. Unfortunately, porous Vycor tubing is not a commercial material and, in any case, it is not available in many pore sizes or different tube dimensions. Corning Inc. produces porous tubing (Code 7930) as an intermediate in the production of nonporous tubing (Code 7900) which has excellent thermal and mechanical properties--similar to those of quartz. Corning Inc. has supplied free of charge tubing of 5 mm ID, 7 mm OD and 40 Å mean pore diameter. They have also provided for a fee tubing of different diameter, wall thickness, and mean pore diameter custom-made for this project.

It turned out that glass blowing operations on tubing of small diameter or small wall thickness was difficult, resulting in frequent failures. Furthermore, the custom made tubing was very expensive, hence, the bulk of the work was carried out with the standard 5 mm ID/7 mm OD/40 Å pore diameter tubing which was rugged and was obtained free of charge.

1.2 Materials

Porous Suppo-t Tubes

Porous Vycor tubing of ten different types varying in dimensions and pore size were obtained from Corning Inc. Among those only three provided useful results in deposition experiments. The dimensions, pore sizes and permeances of these three types are given in Table 1.1 below.

Table 1.1 Properties of Vycor tubing (Corning Code 7930) used to prepare silica membranes.

Code	ID (mm)	OD (mm)	Mean Pore Diameter (Å)	Permeance at 450°C[a] (cm^3(STP)/cm^2-min-atm) H_2	N_2
V1	4.8	7	40	0.4-0.6	0.14-0.22
V2	5	5.66	25	1.05	0.31
V3	2	2.28	30	NA	NA

[a] Variations were observed from batch to batch and among tubes of the same batch.

The tubes were prepared by the glassblower for connection to the CVD reactor as follows. A porous tube segment about 30 cm long was first heated at 100°C for one hour to drive off condensed and physically adsorbed water. After this preliminary heating, each side of the tube was heated gradually in a Bunsen flame to above 1000°C until the porosity collapsed in a section of a few centimeters at each end making that end completely nonporous, while the center section of 10-30 cm length remained porous. Finally short quartz sections 6 mm OD were welded to the nonporous Vycor sections at either end for ready connection to metal tubing using standard Swagelock fittings.

Chemicals

$SiCl_4$ (99.999%), $SiBr_4$ (99%), $AlCl_3$ (99.99%), and $TiCl_4$ (99.9%) were purchased from Aldrich Chemical; BCl_3 (99.999%) from Matheson Gas Products. The chlorosiloxanes $Cl_3SiOSiCl_3$ (hexachlorosiloxane) and $Cl_3SiOSiCl_2OSiCl_3$ (octachlorodisiloxane) were purchased from Huls America, Inc. (formerly Petrarch Systems). High purity N_2, O_2, and H_2 gases were supplied by Matheson Gas Products and further purified by Altech gas purifiers.

1.3 Apparatus and Procedure

Apparatus for Opposing Reactants Deposition

The apparatus for membrane deposition, shown schematically in Figure 1.1 consists of a concentric tube reactor placed in an electrical furnace. The two reactant streams are generated by flowing two carrier N_2 streams, typically at 50 cm^3/min each, through temperature controlled baths of the reactants, e.g. H_2O bath and $SiCl_4$ bath. For Al_2O_3 deposition, an $AlCl_3$ sublimator was used in place of the chloride bubbler, while for B_2O_3 deposition a BCl_3 bottle was used and the gaseous chloride stream was diluted with N_2 to the desired concentration. The temperature of each bath is controlled to achieve the desired mol fraction of the respective reactant. The H_2O-N_2 stream is passed through the reactor shell (annulus) while the $SiCl_4$-N_2 (or $AlCl_3$, $TiCl_4$, BCl_3) stream is passed through the inner, support tube. One can interchange the path of the reactants and pass H_2O through the bore of the support tube and $SiCl_4$ through the annulus between the two concentric tubes. In either case the two reactants diffuse in opposite directions within the tube wall and react to form a solid oxide product, gradually plugging the pores in a narrow layer within the tube wall. The progress of the reaction is followed by periodically interrupting the flow of the reactants, flushing the inner tube and the annulus and measuring the permeance to various gases as described below.

Apparatus for One-Side Deposition

The apparatus for one-sided deposition differs from that of the opposing reactants deposition only in the introduction of the reactants. Figure 1.2 shows introduction of both reactants through the bore of the support tube which was the arrangement used. One can obviously introduce both reactants through the annulus, instead.

The reaction was in all cases conducted at atmospheric pressure both in the bore and in the annulus. For one-sided deposition, atmospheric pressure was maintained in the annulus by flow of pure nitrogen. The concentration of the chloride and water was varied between different series of experiments. Different temperature ranges were investigated for each reactant. Before reaction the support tube was heated at 100 and then 200°C under N_2 flow to remove adsorbed water and then at 600°C under oxygen flow for several hours to remove any adsorbed organic impurities.

Permeation Rate Measurements

The permeation rates of H_2, N_2 and occasionally other gases was measured by maintaining the membrane tube at a fixed pressure of the gas and measuring the flow to the annulus. For sufficiently high flows, the membrane tube was maintained at approximately 3 atmospheres and the flowrate to the annulus was measured using a bubble flowmeter operating at one atmosphere. Permeation rates below the limit measurable by the bubble flowmeter were measured by a sensitive pressure transducer (Baratron) connected to the computer. In this case the membrane tube was maintained at 2 atmospheres under flow while the outer annulus was evacuated and then isolated from vacuum. Using the transient pressure buildup measured by the pressure transducer the membrane permeance was then determined using the following equations (assuming ideal gas behavior):

$$Q\left[\text{cm}^3(\text{STP})/\text{cm}^2\text{-atm-min}\right] = \dot{V}/(A\,\Delta p)$$

$$\dot{V} = K\frac{dp}{dt}$$

where A is the surface of the membrane, Δp the pressure difference across the membrane, dp/dt the rate of pressure rise in the annulus, and K the calibration factor established between the pressure transducer and the bubble flowmeter.

1.4. Results of Membrane Preparation

SiO_2 Membranes

During the first year of the contract, deposition experiments were conducted in the opposing reactants geometry. The results of these depositions are compiled in Table 1.2. At the beginning the temperature of deposition was varied in the range 200-800°C. It was found that deposition is so slow at 200°C that the permeance of the tube remained unchanged after two hours of operation. Even at 600°C deposition for as many as 5 hours was not sufficient for complete pore plugging. Useful results were obtained at 700 and 800°C. At 700°C essentially complete pore plugging was attained within 3 hours although continuing deposition after that time led to further reduction in the permeation rates, especially that of N_2, evidently due to densification and to a possible slow thickening of the already formed layer. At 800°C the reaction is faster requiring about 1.5–2 hours for complete pore plugging. The time required for complete pore plugging by $SiCl_4$ hydrolysis at 700 and 800°C is much longer than the 15–20 minutes required in previous experiments using SiH_4 oxidation at 450°C.

Figure 1.3 shows a typical evolution of the H_2 and N_2 permeance with deposition time at 700 and 800°C (codes 3,4 in Table 1.2). Deposition at 800°C causes a more rapid and pronounced decline in the permeance of nitrogen and a higher H_2:N_2 selectivity (5000 vs 3500 at 700°C deposition). It must be noted that the measurement of very low nitrogen permeances entails significant error because of possible minute leaks in the system. As a result of this error, the true H_2:N_2 selectivities may in some cases be higher than the values listed in Table 1.2.

As shown in Table 1.2, deposition of SiO_2 is much faster in the one-sided geometry than in the opposing reactants geometry. Pore plugging for the V1 tubes (40 Å pore size) requires about 20-30 minutes at 600°C and only 5 minutes or less at 750°C. For he V2 tubes (25 Å pore size) the time was one minute or less. It should be kept in mind that the reaction times listed in Table 1.2 are generally larger than the minimum times required for pore plugging. When the pore plugging time was less than two or three minutes, it was impractical to monitor the progress of deposition by interrupting the reaction, purging, and measuring permeances. Hence, deposition was often continued beyond the point of pore plugging. In the one-sided geometry, continuing the deposition beyond pore plugging will result in slow thickening of the tube wall and decline of the membrane permeance. Although the effect of prolonging the reaction beyond pore plugging was not studied as such, it is expected to be minor as long as the reaction time is no more than two or three times larger than the pore plugging time.

The sharply difference in the times required for one-sided and opposing reactants deposition can be readily understood by the different level of reactant concentrations at the reaction region. In one-sided deposition the reaction region located just below the cylindrical surface bounding the tube wall. At that surface the reactant concentrations are near their free stream values (discounting external mass transfer). In opposing reactants deposition, the concentrations at the reaction region are small fractions of their boundary values because of the two diffusion gradients. As a result of the lower concentration, the reaction rate in the opposing reactant geometry is lower and, hence, the reaction region and the resulting deposit layer are thicker than in the one-sided geometry.

TiO_2, Al_2O_3, and B_2O_3 Membranes

Table 1.3 shows the properties of membranes prepared by the deposition of TiO_2, Al_2O_3, and B_2O_3 layers on porous Vycor tubes (V1 type). It should be noticed that all TiO_2 and Al_2O_3 membranes were prepared in the opposing reactants geometry. Several attempts made to prepare such membranes in the one-sided geometry were unsuccessful,

with little or no change in the permeance of nitrogen--or hydrogen--taking place in several hours of deposition. Boron oxide membranes, however, could be prepared in both deposition geometries although most preparations were carried out in the opposing reactants geometry. The failure of deposition in the one-sided geometry to produce permselective layers will be discussed in a later section.

Concerning now the permeation properties of these various oxides, we note that the TiO_2 membranes deposited at 450 and 600°C had hydrogen permeance only moderately lower than the SiO_2 membranes prepared in the opposing reactants geometry. The H_2:N_2 permeance ratio of the TiO_2 membranes was in the range 200-1500 depending on deposition time and temperature. Figure 1.4 shows the evolution of hydrogen and nitrogen permeances during the deposition reaction at 450 and 600°C. The TiO_2 membranes prepared at 800°C had much lower hydrogen permeance and selectivity than the SiO_2 counterparts, indicating some structural difference in the TiO_2 layer prepared at the higher temperatures. Below 600°C it is possible that TiO_2 is stabilized by the surrounding SiO_2 matrix (of the Vycor support) to either an amorphous phase or to anatase, whereas at higher temperatures transition to the denser rutile phase might take place.[1]

Alumina membranes were prepared at 450, 700 and 800°C in the opposing reactants geometry. The results are summarized in Table 1.3 and Figure 1.5. The hydrogen permeance of the Al_2O_3 membranes prepared at 700 and 800°C is substantially below that of the SiO_2 membranes. The H_2:N_2 permeance ratio is below 400, also well below that of the SiO_2 membranes. Somewhat better H_2:N_2 ratio was obtained when the Al_2O_3 membranes prepared at 450 were subsequently annealed at 700°C. However, the hydrogen permeance did not improve by this annealing.

Boron oxide layers could be deposited over a wide temperature range (50-800°C). Deposition above 500°C produced membranes with low hydrogen permeance. Membranes prepared by deposition at temperatures between 100 and 450°C had hydrogen permeance as high as 0.2 cm^3/cm^2-min-atm at 450°C and 0.03 cm^3/cm^2-min-atm at 150°C. At 150°C the

hydrogen permeance of the SiO_2 membranes was negligible. Unfortunately, the hydrogen permeance of the B_2O_3 membranes declined significantly upon annealing above 500°C. Figure 1.6 shows the evolution of H_2 and N_2 permeance at 150°C during deposition at the same temperature. Boron oxide membranes were subject to attack by water. Upon exposure to the laboratory atmosphere for several weeks, they developed boric acid whiskers and eventually cracked. Evidently, capillary condensation of water in the small Vycor pores and the smaller pores partly coated by B_2O_3 caused the conversion of B_2O_3 to $B(OH)_3$ causing the mechanical failure. Figure 1.7 contains several Arrhenius plots of the hydrogen permeance of a B_2O_3 deposited at 150°C, subsequently annealed and finally exposed to the laboratory atmosphere for 23 days.

1.5 Membrane Characterization

Membrane characterization was carried out by scanning electron microscopy (SEM) and electron microprobe analysis (EMA). SEM was conducted with a CamScan electron microscope operating at 20 kV and with resolution of 500 Å. Both cylindrical surfaces (the side of the chloride flow) and cross sections of membrane tubes were examined. To examine a tube cross section the sample was cut, cast in epoxy resin, polished and coated with carbon or gold. In addition to SEM, tube cross sections were also examined by a Jeol 733 Superprobe electron microprobe by wavelength dispersive spectroscopy to obtain the elemental composition as a function of radial distance.

Examination of Tube Cross Sections

Tube cross sections after CVD of SiO_2, TiO_2 and Al_2O_3 were examined by SEM and EMA. Examination of SiO_2 deposit layers turned out to be difficult when a focused electron beam was used because of sample burning. By defocusing the electron beam it was possible to obtain microprobe traces on SiO_2 layers but at lower resolution. Al_2O_3 and TiO_2 layers were easier to characterize.

An SEM micrograph of an Al_2O_3 membrane obtained by opposing reactants deposition is shown on Figure 1.8. The darker region near the inner radius signifies the alumina layer, while the white line at the end of that region is an artifact due to polishing. Figure 1.9 shows the EMA trace of the alumina layer shown in Figure 1.8. The trace shows a gradually rising concentration of Al_2O_3 followed by a steep drop. The Al_2O_3 deposit covers a region of almost 90 μm but the much narrower peak region is where Knudsen diffusion is completely disrupted and transport takes place by activated diffusion in the dense layer. Figure 1.10 shows the development of the deposit density profile during Al_2O_3 deposition in the opposing reactants geometry. Early during deposition the profile is monotonically declining, but later on its develops a maximum which sharpens until pore plugging when the reaction stops.

As stated earlier, the EMA of SiO_2 layers required defocusing of the electron beam and hence gave relatively low resolution, about 5 μm, as opposed to the approximately 1 μm resolution employed for the Al_2O_3 layers. Figure 1.11 shows the EMA trace of a SiO_2 layer deposited in the opposing reactants geometry. This particular deposit layer was very wide and because of the lower resolution it does not show the sharp peak shown in the previous EMA scans. Figure 1.12 shows the EMA scan of a SiO_2 layer deposited in one-sided geometry on a Vycor tube with 120 μm mean pore diameter (V2, defined in Table 1.1) All other EMA traces shown here were obtained for deposition on support tubes with 40 Å mean pore diameter (V1, defined in Table 1.1). As expected, the profile is monotonically declining and penetrates about 70 μm from the chloride side. Complete disruption of Knudsen diffusion takes place only over a much thinner layer at the inner tube radius (zero distance from chloride flow). The thickness of this hydrogen permselective layer cannot be measured from the EMA scans because of the low resolution. EMA scans of two SiO_2 membranes prepared by one-sided deposition on Vycor tubes with 40 Å mean pore diameter are shown in Figure 1.13. The main difference between the traces of Figures 12 and 13 is the much shallower deposit penetration in the latter. Although different

reactant concentrations were used in these depositions, the difference in the depth of penetration is primarily due to the different pore size of the support tubes.

Examination of Cylindrical Surface (side of reactants flow)

The inside cylindrical surface exposed to the $SiCl_4$, H_2O reactants was examined by SEM. Figure 1.14a shows a micrograph of a Vycor tube before deposition. Although these tubes have 40 Å mean pore diameter as determined by nitrogen adsorption, the pore mouths seen on the micrograph are much larger, perhaps in the range 200-300 Å. It appears that in the leaching process used to prepare the Vycor tubes, larger pores are developed in a thin skin near the external surface. Transmission electron micrographs (not shown here) verify that the pores in the bulk of the Vycor have mean pore diameter of about 40 Å. Figure 1.14b shows a micrograph of a surface after deposition with low concentration of $SiCl_4$. Comparison of Figures 1.14a and 1.14b reveals that deposition does not change significantly the texture of the surface and suggests that the deposit layer does not extend outside of the porous matrix. To investigate the evolution of the deposit layer when deposition is continued beyond the time of pore plugging, we prolonged deposition under the conditions of Figure 1.14b, for 15 and 35 additional minutes after pore plugging (30 and 50 minutes of total deposition time). Examination of the surface by SEM (Figure 1.15) indicates that after pore plugging the deposit continues to grow outside of the pore matrix.

The influence of the $SiCl_4$ reactant concentration on the morphology of the deposit is revealed by comparison of Figure 1.16 with Figure 1.14b. Figure 1.16 shows the micrograph of the surface after deposition with 8.7% $SiCl_4$, 13% H_2O for 30 minutes (immediately after pore plugging). With both reactants at high concentration, a pronounced surface roughness is observed indicating the adherence on the surface of particles which are too large to enter into the pores. Pore plugging still takes place by penetration and heterogeneous reaction of $SiCl_4$, and possibly some oligomers, on the internal pore surface area. Since the monomer concentration is reduced by the homogeneous reactions,

the time for pore plugging is increased to 30 minutes as compared to the 15 minutes that were required for the conditions of Figure 1.14b.

1.6 Discusion

The mechanism of SiO_2 deposition by $SiCl_4$ hydrolysis has been discussed in two recent publications deriving from this project.[1,2] The reaction takes place homogeneously and heterogeneously. In opposing reactants deposition, the reaction region is wholly inside the porous matrix of the support where because of the low reactant concentrations and the large surface area per unit volume deposition occurs by heterogeneous reaction. Any dimers or oligomers generated homogeneously would also react with the surface before diffusing outside. In one-sided deposition, the maximum concentration of reactants is in the bore (or in the annulus) so that homogeneous reaction as well as heterogeneous reaction take place. If the homogeneous reaction is too fast, the reactant $SiCl_4$ becomes largely depleted before it can diffuse inside the pores. This seems to be the case with the $TiCl_4$-H_2O and $AlCl_3$-H_2O reactions where deposition fails to plug the pores of the support. In the case of SiO_2 deposition under the temperatures and reactant concentrations employed the homogeneous $SiCl_4$-H_2O reaction is not fast enough to exhaust the reactants and prevent pore plugging. However, at $SiCl_4$ pressures above about 10% the particles generated by the homogeneous reaction adhere to the bore surface and can cause thermal stresses upon cooling and reheating as will be discussed in the following chapter.

While penetration of the reactants into the pore matrix is essential in one-sided deposition, the depth of penetration must be kept as small as possible to obtain a thin membrane and high hydrogen permeance. This depth of penetration is approximately given by

$$\delta = \left(\frac{\mathcal{D}_0}{k\,[OH]_0 S} \right)^{1/2}$$

where k is the rate constant for the reaction of $SiCl_4$ with surface -OH groups, $[OH]_0$ is the initial surface concentration of -OH groups, S is the pore surface area per unit volume, and

$\mathscr{D}_0$ is the initial (Knudsen) effective diffusivity. For a given support material the penetration δ may be decreased by increasing the rate constant k and/or decreasing the diffusion coefficient $\mathscr{D}_0$. The reaction rate may be increased by increasing the temperature. Raising the temperature, however, has the undesirable effects of eliminating surface -OH groups (decreasing $[OH]_0$), intensifying the homogeneous reaction, and above 900°C, collapsing the porous structure. It appears that the optimal deposition temperature by the $SiCl_4$-H_2O reaction is about 750°C.

In section 1.2 we listed two silicon reagents, in addition to $SiCl_4$, which were used in a limited number of preparation experiments. These reagents, $Cl_3SiOSiCl_3$ (hexachlorosiloxane) and $Cl_3SiOSiCl_2OSiCl_3$ (octachlorodisiloxane) have higher k (more Cl groups) and lower $\mathscr{D}_0$ (higher molecular weight) than $SiCl_4$, and as a result they should have smaller penetration depth δ. Only slight improvement of hydrogen permeance was obtained with these reagents, but there is some scope for additional improvement.

A more significant variation that was briefly explored was the use of Vycor support tubes of smaller pore diameter. Decreasing the pore diameter increases $[OH]_0$ (more surface area) and decreases $\mathscr{D}_0$ resulting, again, at a smaller penetration depth δ. Because of the lower $\mathscr{D}_0$, the thickness of the tube wall should also be decreased, otherwise the larger resistance of the untreated support tube would limit the advantage of a thinner deposit layer.

Literature Cited

1. Tsapatsis, M., Kim, S., Nam, S-W, and Gavalas, G. R., *I&EC Research* **30**, 2152 (1991).

2. Tsapatsis, M., and Gavalas, G. R., *AIChE J.* **38**, 847 (1992).

Table 1.2 Properties of silica membranes prepared under different conditions.

Code	Support Tubing	Reaction Geometry	Reactants (mol fraction)		Reaction Temp.,°C	Reaction time, min	Gas Permeance $cm^3(STP)/cm^2$-min-atm at 450°C		Gas Permeance $cm^3(STP)/cm^2$-min-atm at deposition temperature	
							H_2	N_2	H_2	N_2
			$SiCl_4$	H_2O						
3	V1	opposing	0.3	0.07	700	240	0.07	$2x10^{-4}$		
4	V1	opposing	0.3	0.07	800	100	0.1	0.2		
5	V1	opposing	0.3	0.07	800	20	0.09	0.8		
6	V1	opposing	0.1	0.08	800	90	0.09	0.7		
7	V1	opposing	0.19	0.08	800	90	0.07	0.4		
8	V1	opposing	0.3	0.08	800	90	0.12	3		
9	V1	opposing	0.3	0.08	800	90	0.05	0.8		
10	V1	opposing	0.15	0.12	750	120	0.06	8		
11	V1	one-sided	0.125	0.06	600	20			0.29	$5x10^{-4}$
12	V3	one-sided	0.125	0.06	600	25			0.53	4
13	V1	one-sided	0.125	0.06	600	40			0.41	12
14	V1	one-sided	0.02	0.025	600	55	0.35	5	0.53	25
15	V1	one-sided	0.02	0.025	600	35	0.21	0.3		
16	V1	one-sided	0.027	0.01	600	42	0.26	5	0.37	20
17	V1	one-sided	0.027	0.13	600	20	0.22	2	0.36	10
18	V1	one-sided	0.027	0.07	600	25	0.23	7	0.37	30
19	V1	one-sided	0.087	0.01	600	35	0.27	6	0.40	20
20	V1	one-sided	0.027	0.13	750	5	0.25	5	0.33	7
21	V1	one-sided	0.15	0.04	800	25	0.09	0.8	0.29	15
22	V1	one-sided	0.15	0.04	600	10	0.28	0.7	0.43	7
23	V1	one-sided	0.15	0.04	400	95	0.08	5	0.07	40
24	V1	one-sided	0.02	0.06	750	4	0.22	9	0.27	10
25	V2	one-sided	0.02	0.06	750	0.8	0.26	30	0.40	16
26	V2	one-sided	0.02	0.06	750	3			0.38	8
			dimer	H_2O						
27	V1	one-sided	0.007	0.05	700	5	0.21	40	0.26	30
28	V1	one-sided	0.007	0.22	700	22			0.30	22
29	V2	one-sided	0.007	0.05	700	2	0.52	13		
			trimer	H_2O						
30	V1	one-sided	f	0.22	700	11			0.45	5.5

Table 1.3 Properties of TiO_2, Al_2O_3 and B_2O_3 membranes prepared under different conditions. Support tubes in all cases were of type VI (see Table 1.1).

Code	Reaction Geometry	Reactants (mol fraction)		Reaction temp, °C	Reaction time, min	Gas Permeance $cm^3(STP)/cm^2$-min-atm at 450°C		Gas Permeance $cm^3(STP)/cm^2$-min-atm at deposition temperatures	
						H_2	N_2	H_2	N_2
		$TiCl_4$	H_2O						
T1	opposing	0.20	0.12	450	35	0.09	$5.9x10^{-4}$	0.09	$5.9x10^{-4}$
T2	opposing	0.20	0.12	450	60	0.06	0.4	0.06	0.4
T3	opposing	0.20	0.12	600	35			0.17	3.8
T4	opposing	0.20	0.12	600	60			0.08	0.59
T5	opposing	0.20	0.12	800	50			0.02	11
		$AlCl_3$	H_2O						
A1	opposing	0.20	0.07	800	120	0.03	5.5	0.02	2.8
A2	opposing	0.20	0.07	450	60	0.004	0.24	0.01	0.24
A3	opposing	0.20	0.07	450	30	0.03	0.63	0.03	0.63
A5	opposing	0.20	0.07	700	60	0.03	3.2		
		BCl_3	H_2O						
B1	opposing	0.10	0.10	450	105	0.11	0.12	0.1	0.2
B2	one-sided	0.10	0.10	500	10			0.3	4
B3	opposing	0.10	0.10	150	90			0.03	0.5
T6	opposing	0.10	0.20	600	45			0.194[a]	7.3[a]
T7	opposing	0.10	0.20	450	45			0.145[a]	5.4[a]
T8	opposing	0.10	0.20	200	35			0.174[a]	5.7[a]

[a] at 600°C

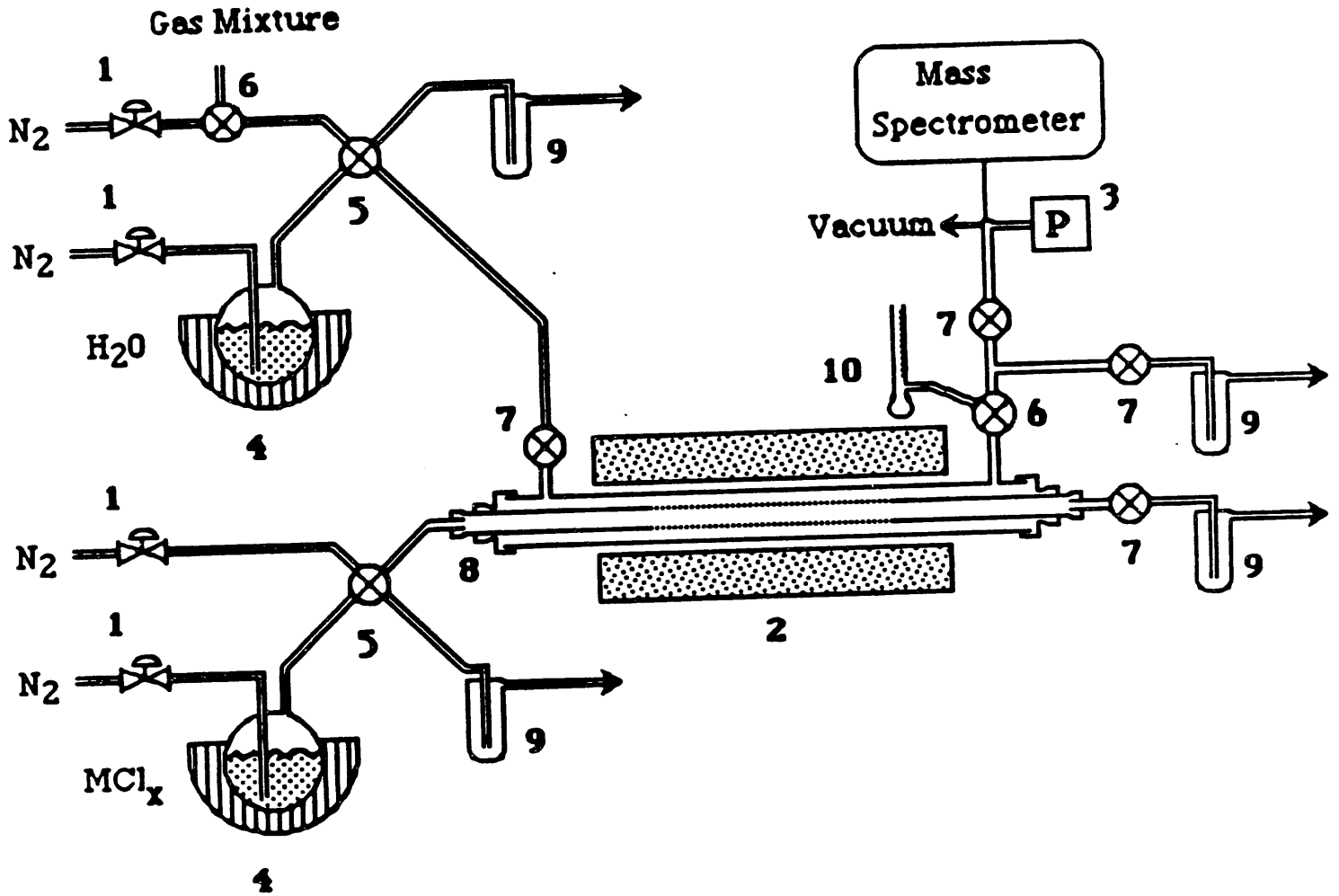

Figure 1.1. Apparatus for membrane CVD in the opposing reactants geometry.

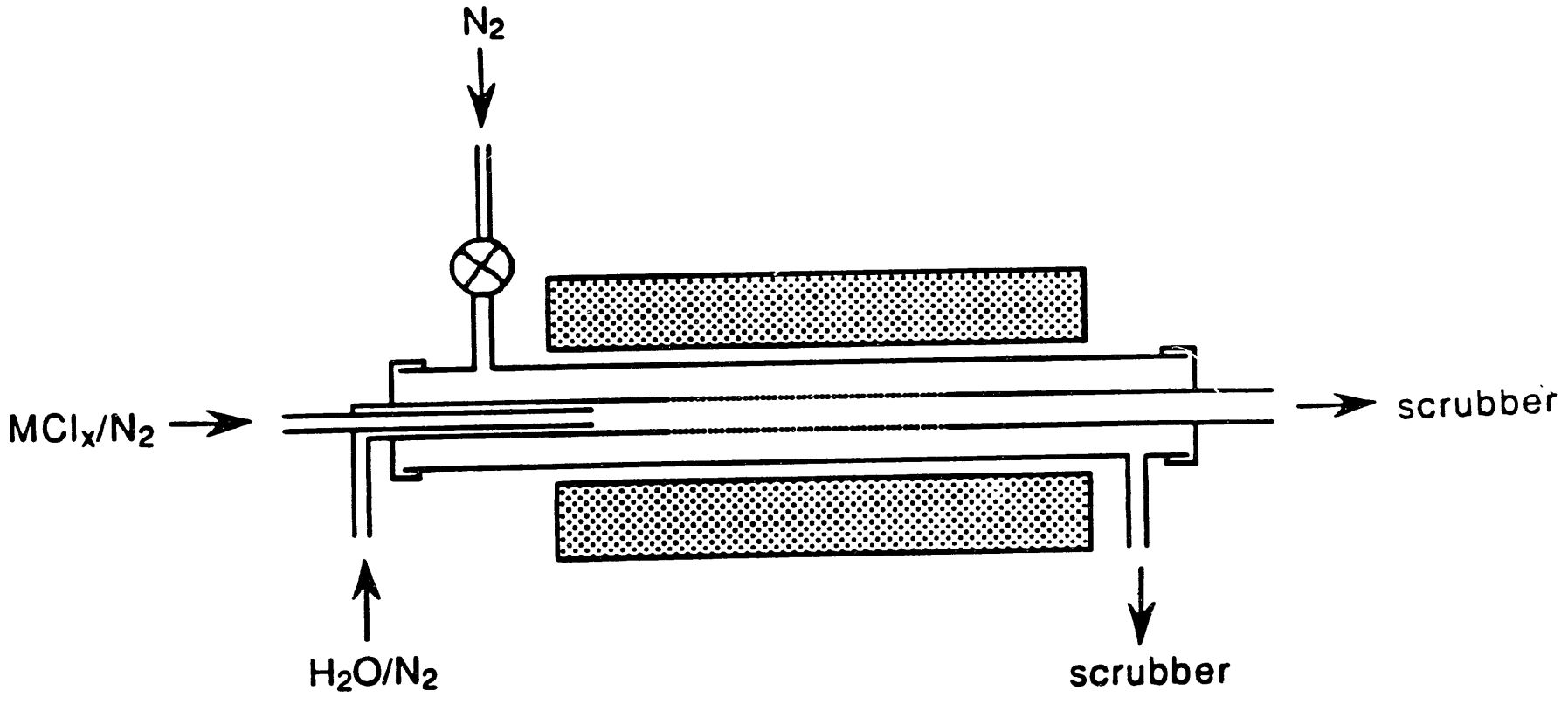

Figure 1.2. Membrane CVD in the one-sided geometry.

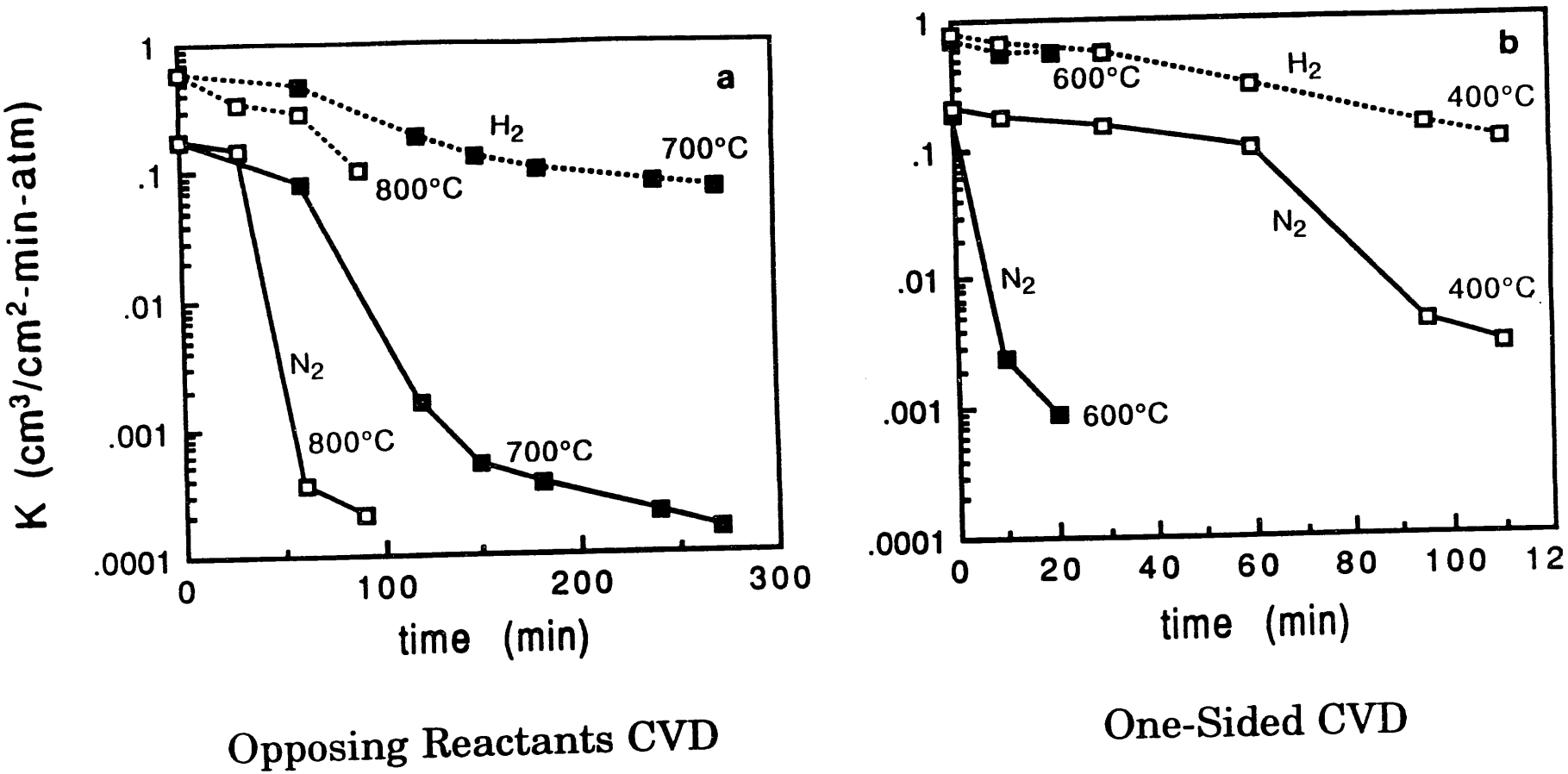

Figure 1.3. Evolution of H_2 and N_2 permeances during SiO_2 membrane CVD in the opposing reactants and one-sided geometries.

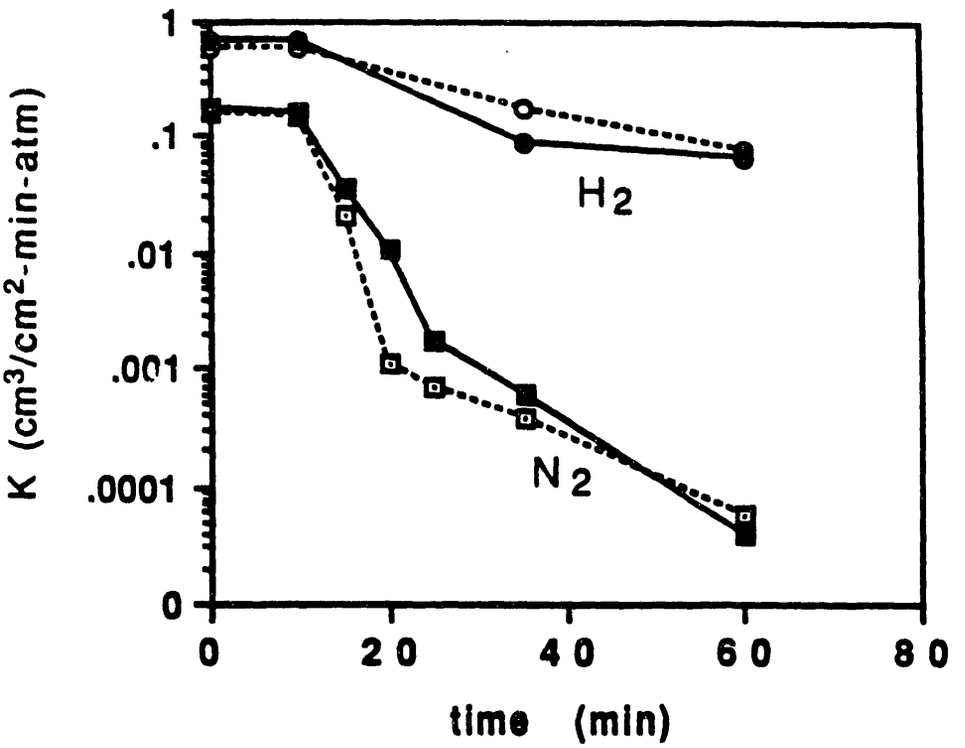

Figure 1.4. Nitrogen (□,■) and hydrogen (○,●) permeation coefficients of TiO_2 membranes during deposition at 450°C (——) and 600°C) (- - -). Reactants: 20% $TiCl_4$-N_2 and 12% H_2O-N_2.

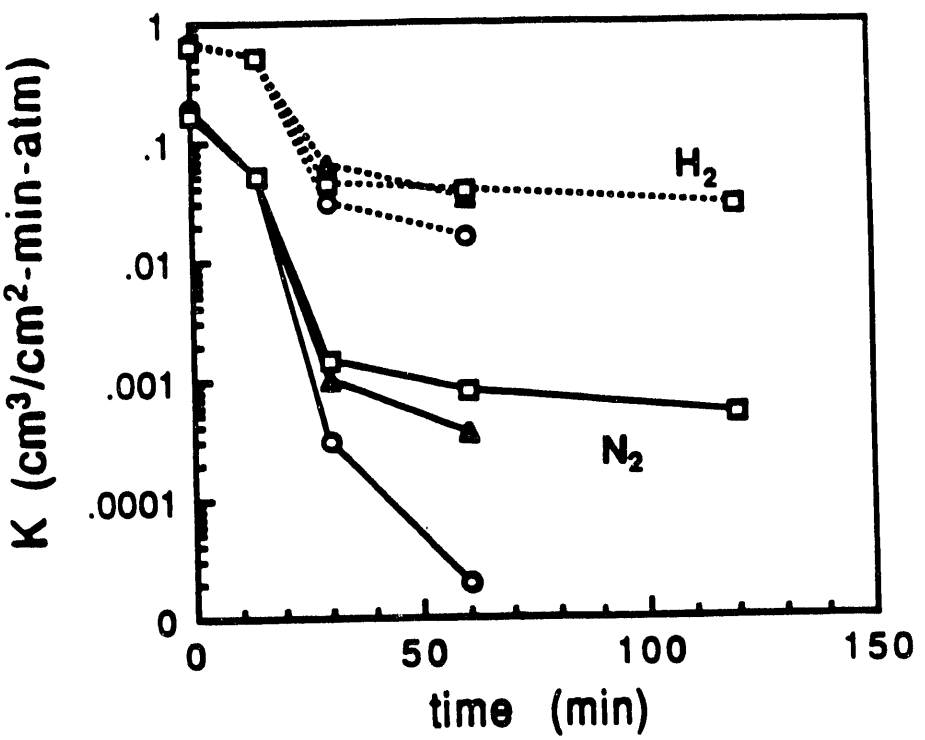

Figure 1.5. Permeation rate coefficients measured at deposition temperatures for hydrogen (- - -) and nitrogen (——) versus time of $AlCl_3 + H_2O$ reaction at 450°C (o), 700°C (Δ), 800°C (□). Reactant streams were 7% H_2O-N_2 and 20% $AlCl_3$-N_2 in opposing reactants geometry.

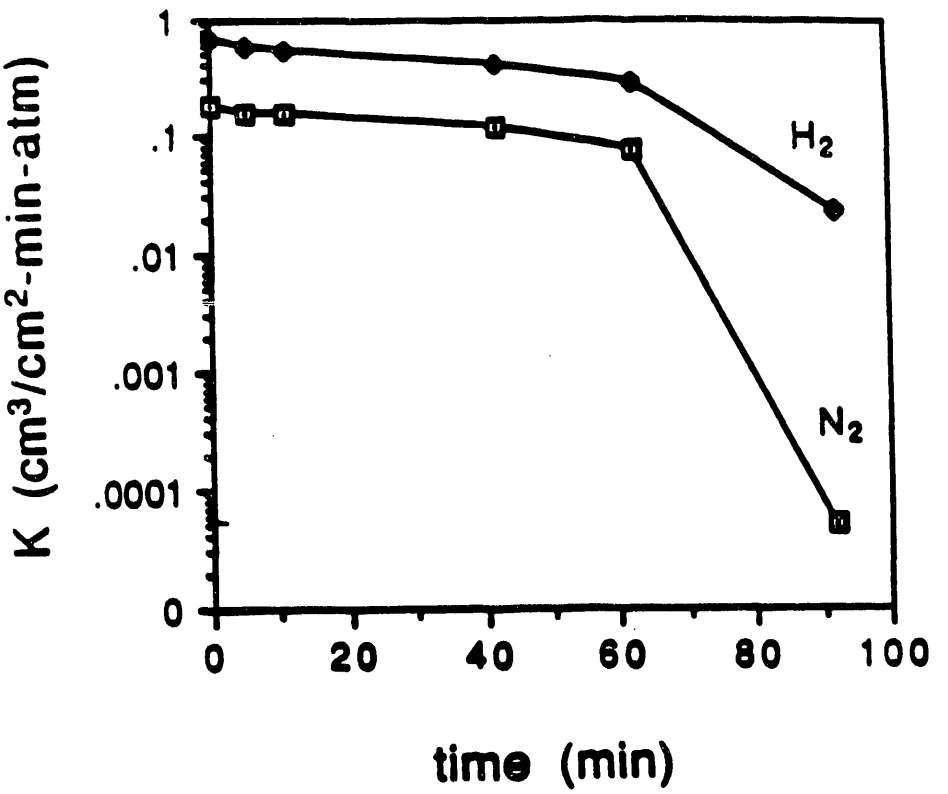

Figure 1.6. Hydrogen and nitrogen permeation coefficients at 150°C during deposition of B_2O_3 at 150°C in opposing reactants geometry. Reactant streams: 10% BCl_3-N_2 and 10% H_2O-O_2.

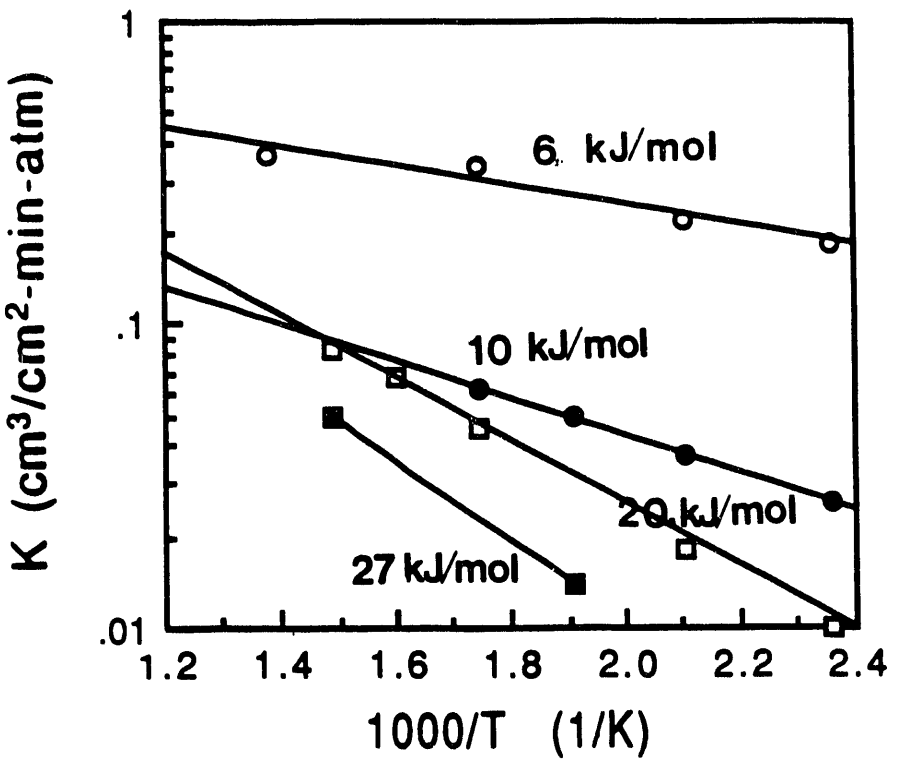

Figure 1.7. Hydrogen permeability coefficients of a B_2O_3 membrane deposited at 150°C and annealed under dry N_2 at 400°C overnight (■), 300°C (□) overnight, 150°C overnight (●) and exposed to laboratory air at room temperature for 23 days (o). Calculated activation energies are given on the figure.

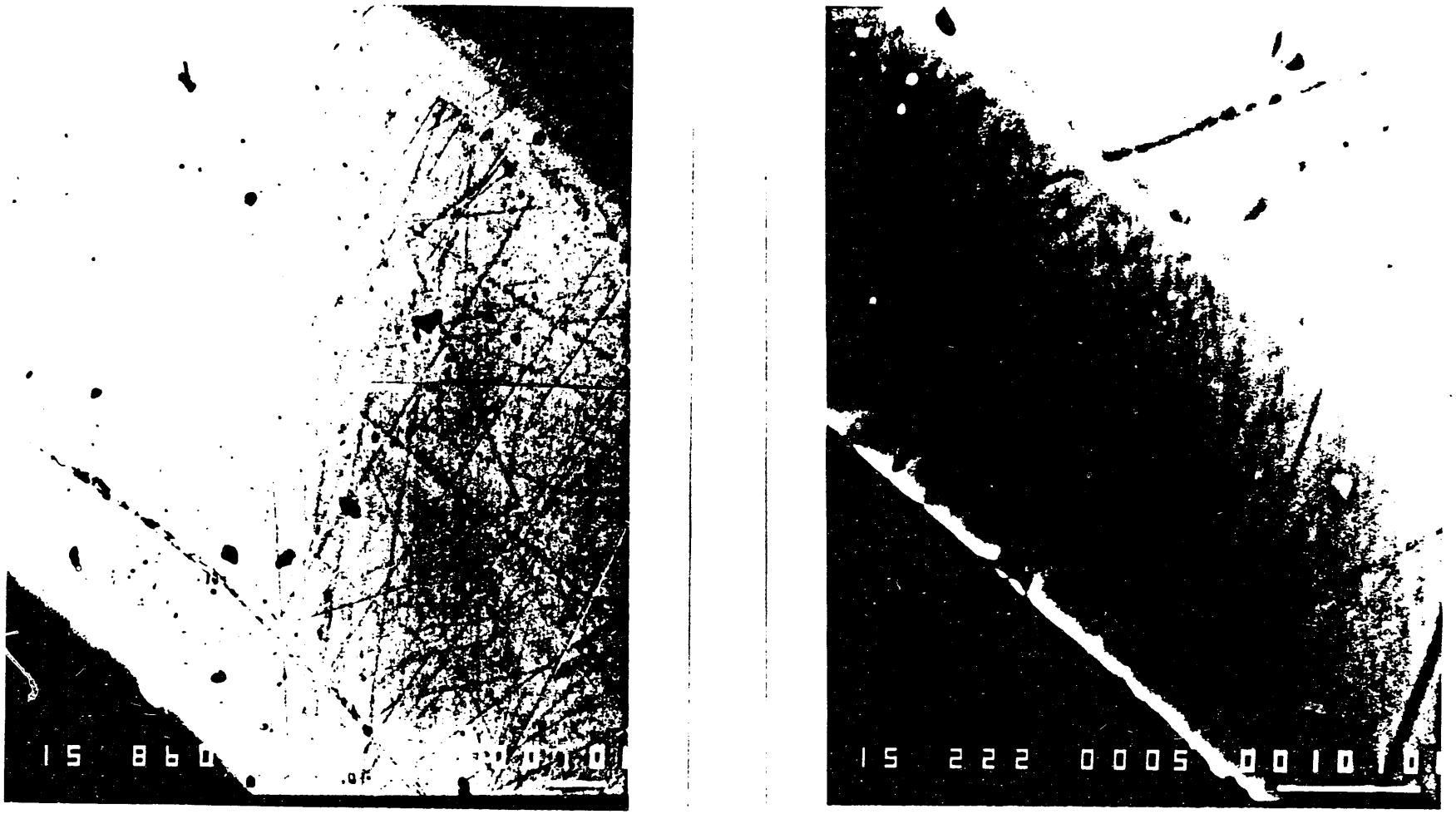

Figure 1.8. SEM in two magnification of the cross section of an Al_2O_3 membrane prepared at 800°C by opposing reactants deposition with 20% $AlCl_3$-N_2, 7% H_2O-N_2.

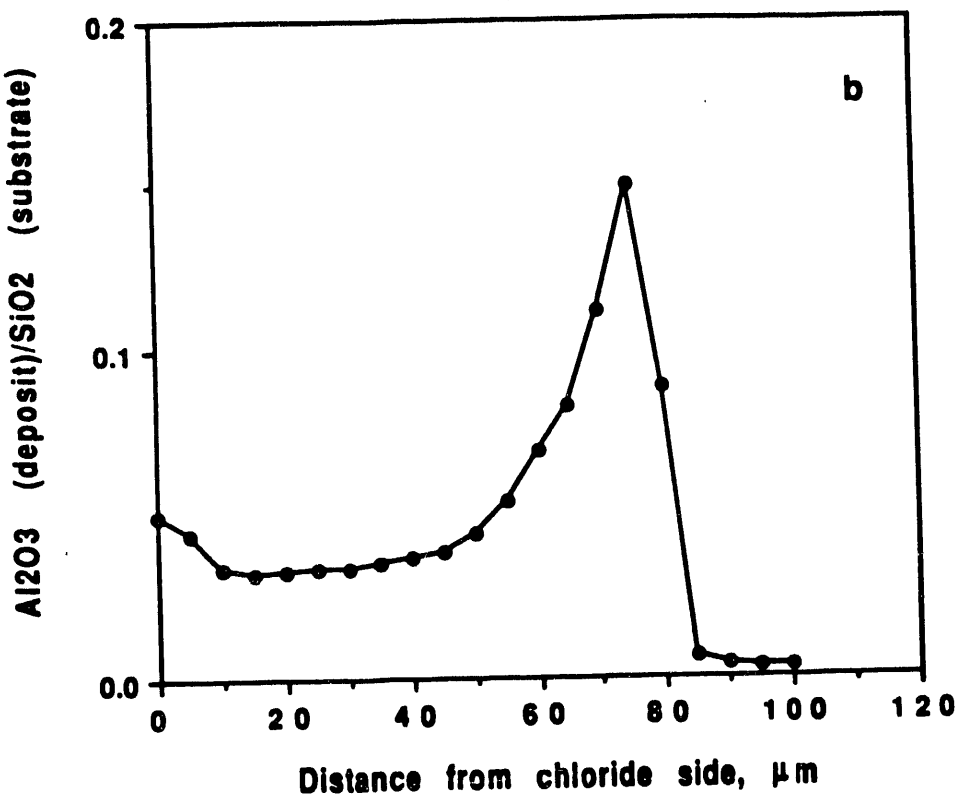

Figure 1.9. EMA trace of the Al_2O_3 layer shown in Figure 1.8.

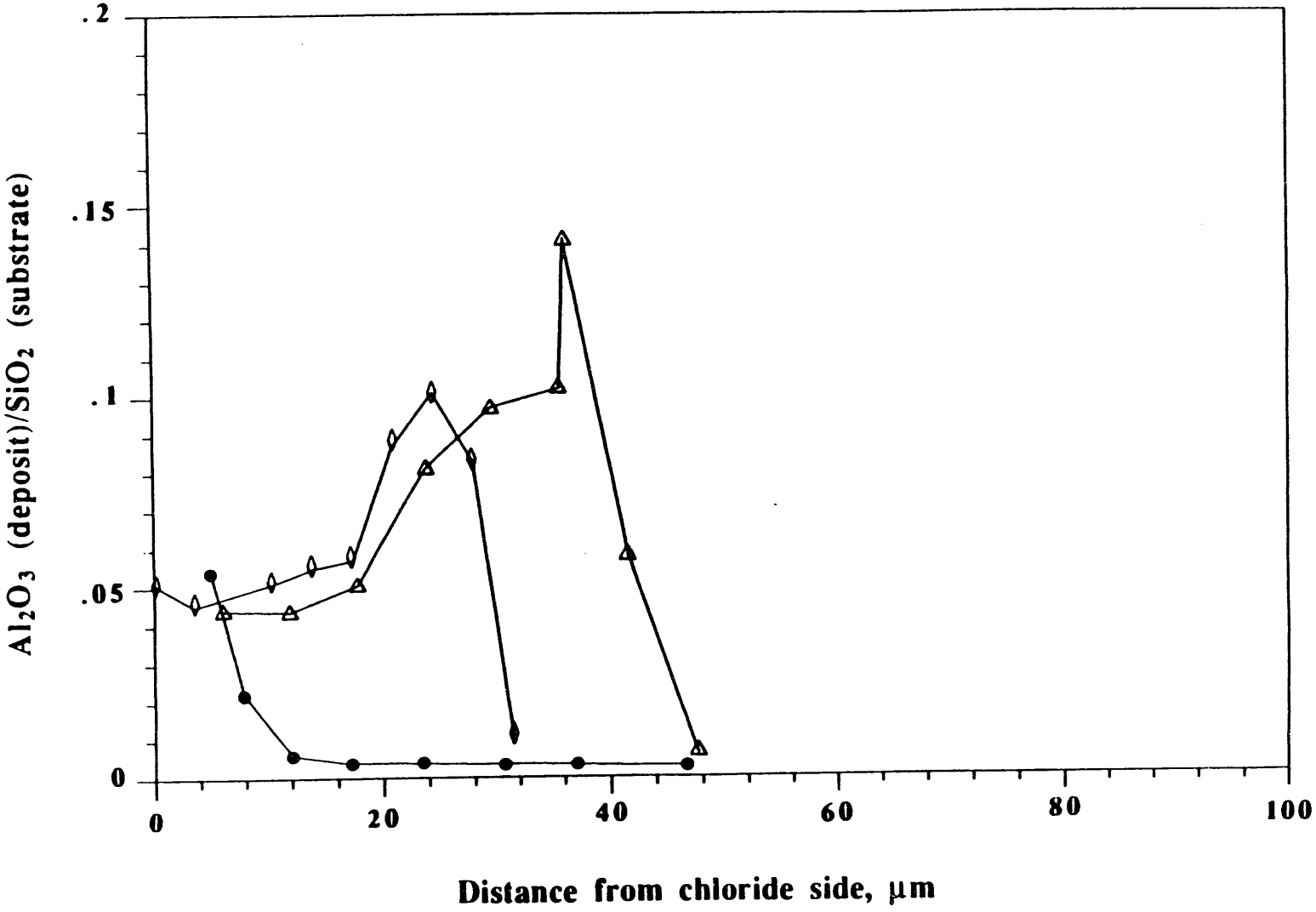

Figure 1.10. EMA of Al_2O_3 membrane cross sections at different times during deposition in the opposing reactants geometry. (450°C with 20% $AlCl_3$-N_2, 7% H_2O-N_2). Deposition times are 3 min (●), 10 min (◊), 15 min (Δ).

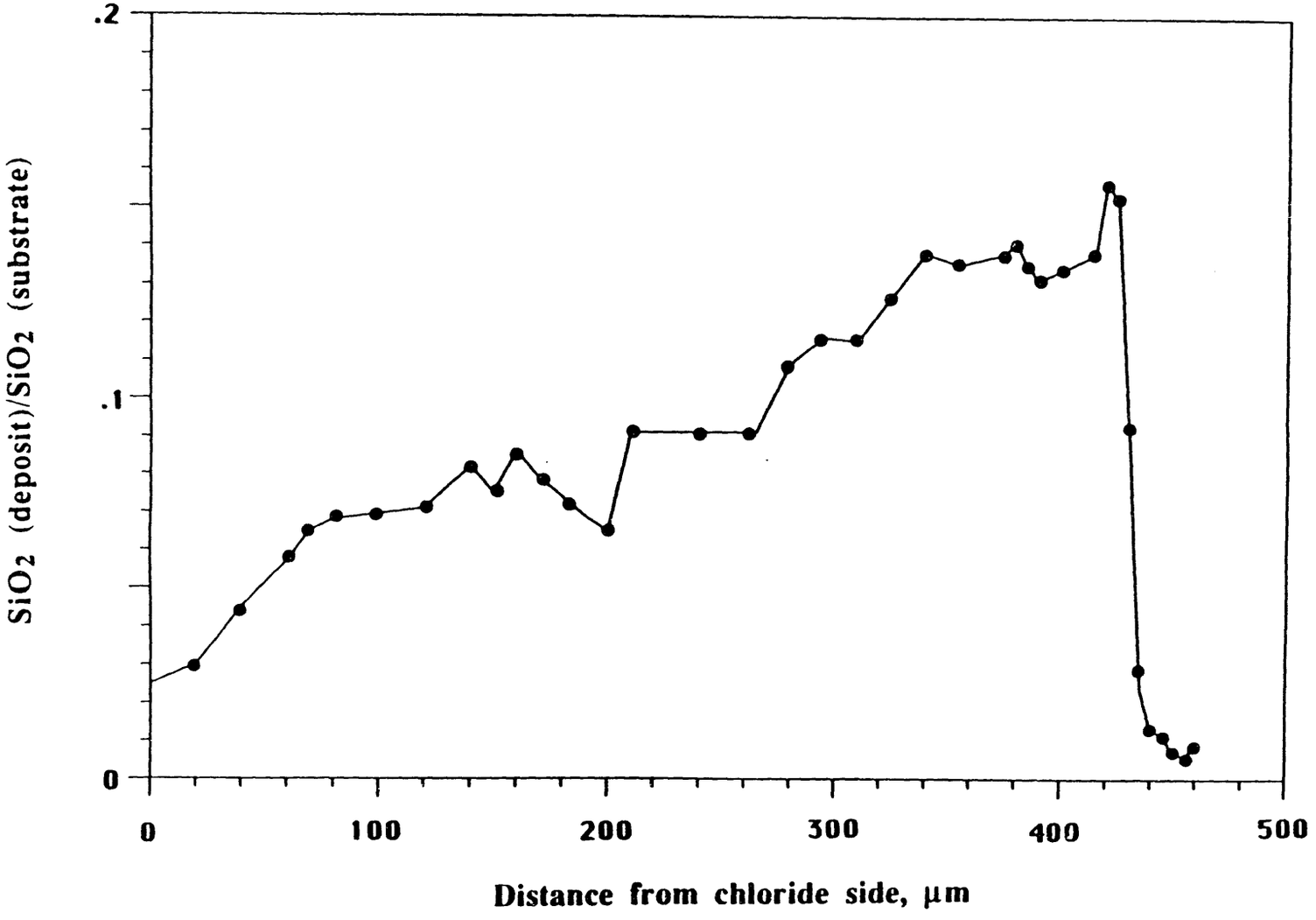

Figure 1.11. EMA scan of a SiO_2 layer deposited in the opposing reactants geometry using 30% $SiCl_4$-N_2, 7% H_2O-N_2 for one hour.

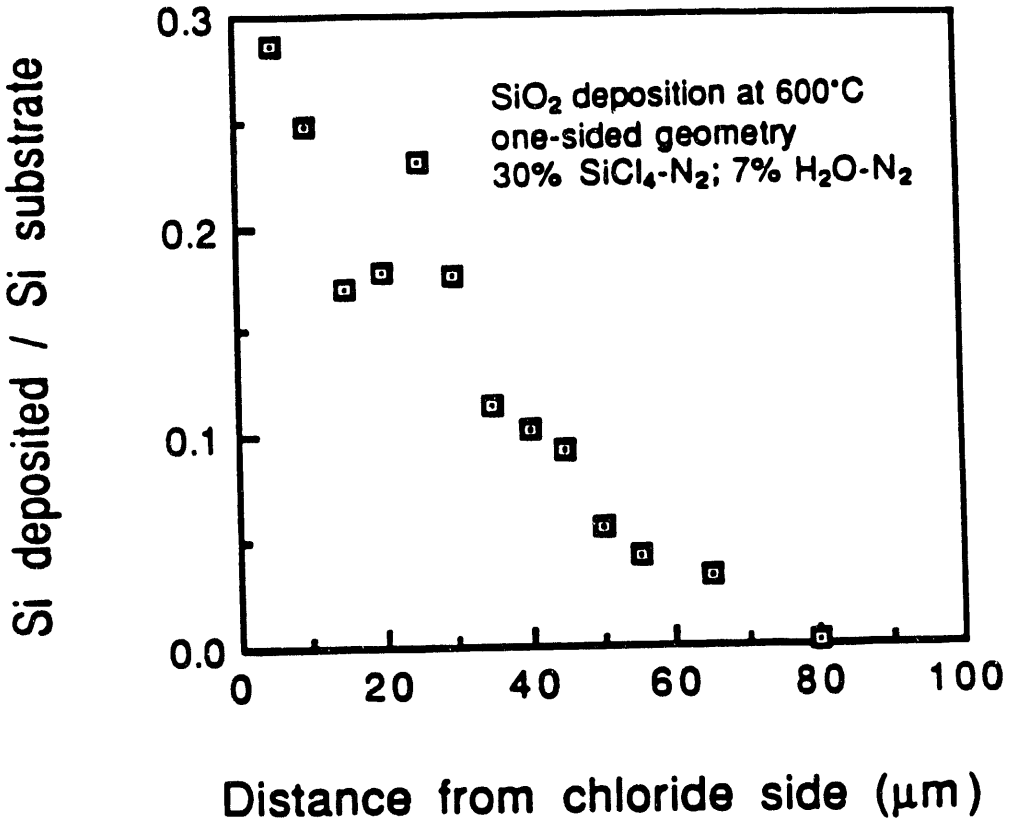

Figure 1.12. EMA of a SiO_2 layer deposited in one-sided geometry on a Vycor tube of 120 Å mean pore diameter.

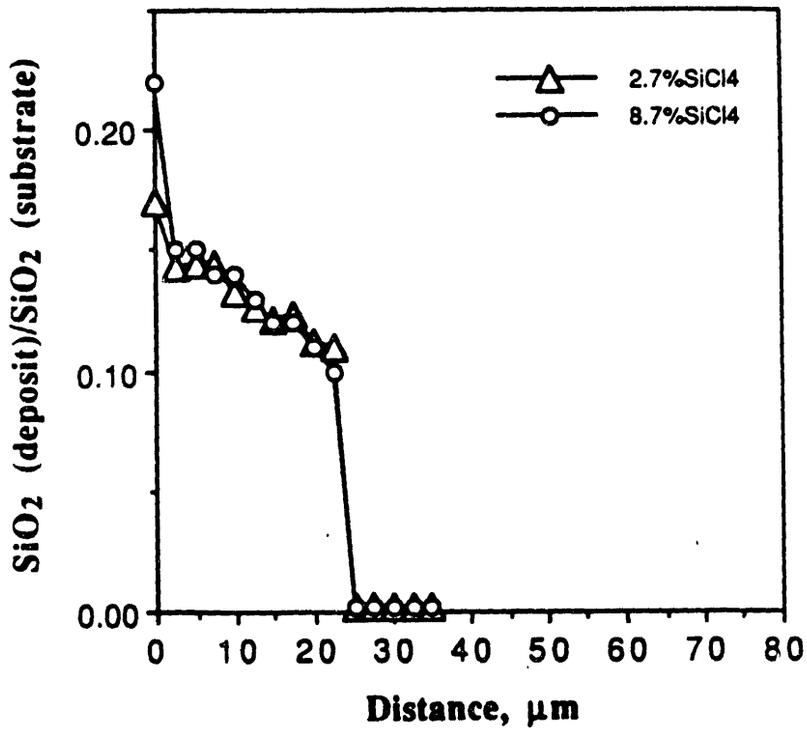

Figure 1.13. EMA of silica membranes deposited at 600°C in OSG with 13% H_2O.

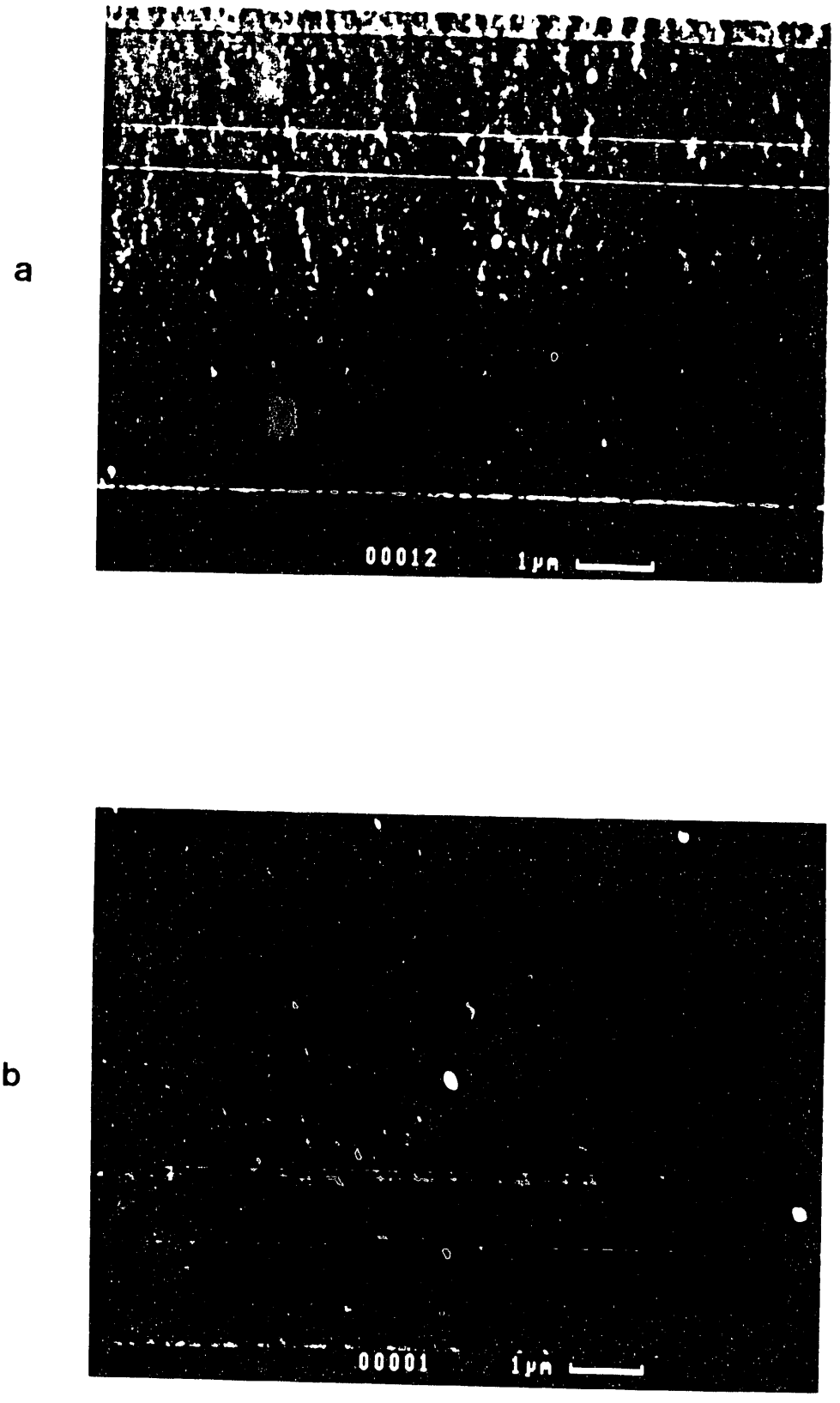

Figure 1.14. SEM micrographs of the bore surface of a Vycor tube (a) before deposition (b) after deposition in one-sided geometry with 2.7% $SiCl_4$ and 13% H_2O at 600°C for 15 minutes.

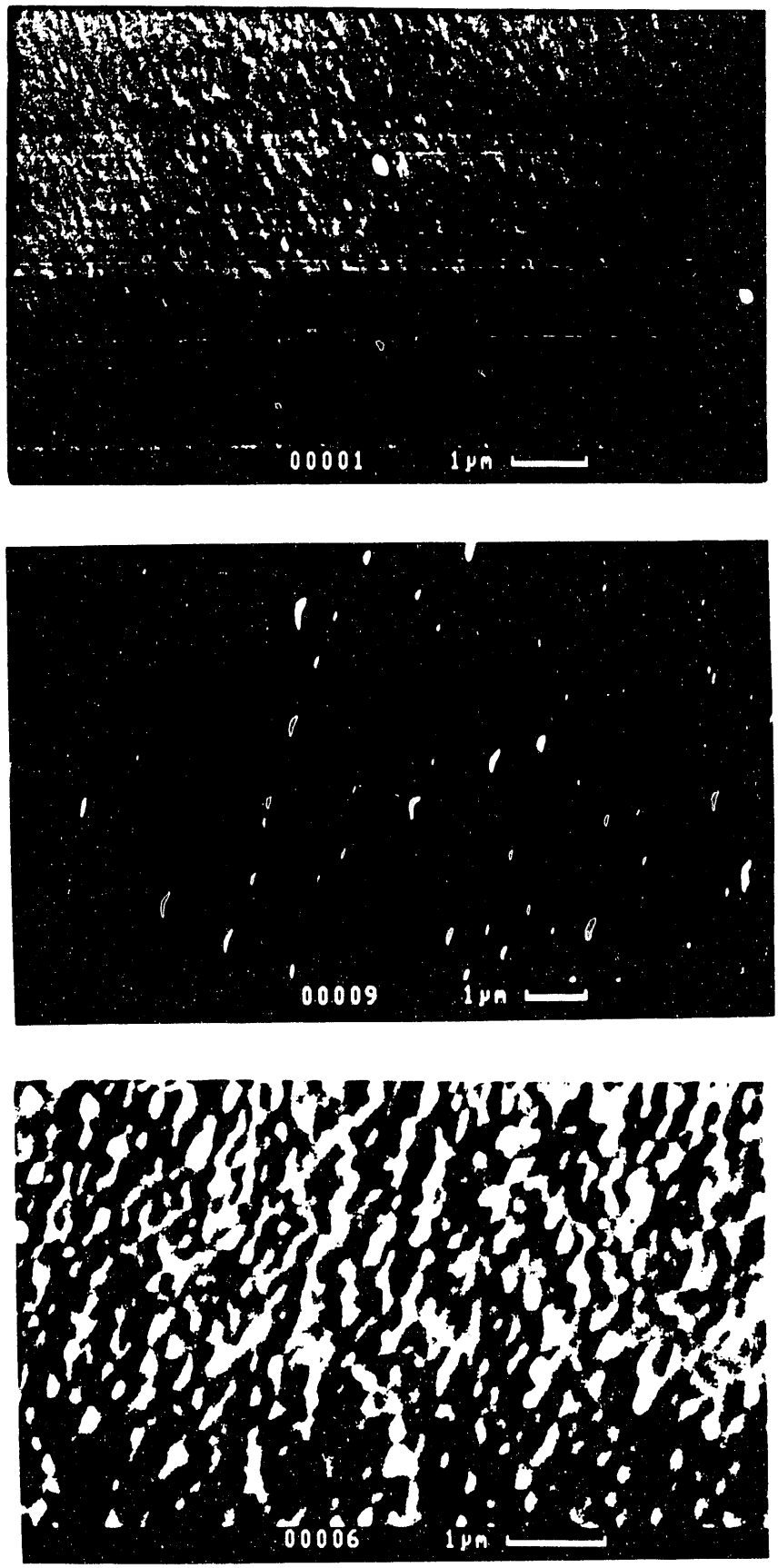

Figure 1.15. SEM micrographs of the bore surface of a Vycor tube after SiO_2 deposition with 2.7% $SiCl_4$ and 13% H_2O at 600°C. Deposition time was 15 minutes (a), 30 minutes (b), 50 minutes (c).

a

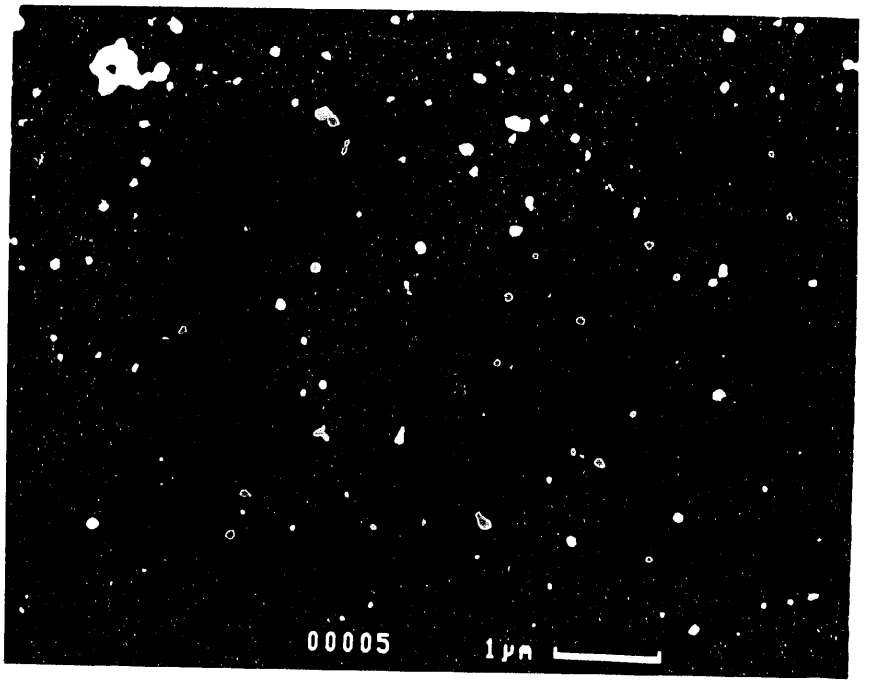

b

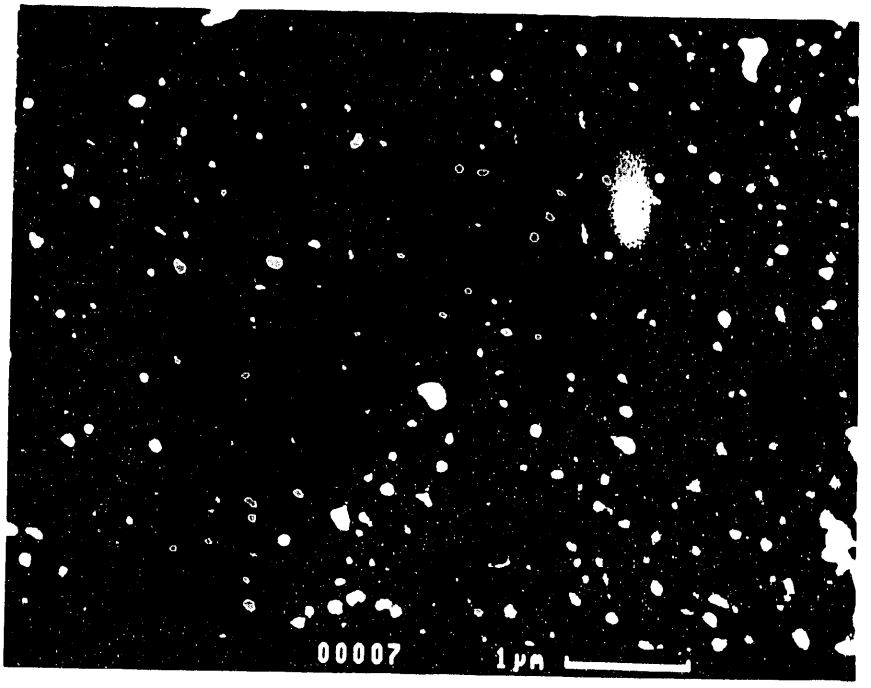

Figure 1.16. SEM micrographs of the bore surface of a Vycor tube after SiO_2 deposition using 8.7% $SiCl_4$ and 13% H_2O at 600°C for 30 minutes (immediately after pore plugging).

Chapter 2

Membrane Stability Testing

2.1 Introduction

Silica films produced by silane (SiH_4) oxidation are known to undergo densification upon prolonged annealing at high temperatures.[1,2] In the presence of water vapor this densification is more severe such that heating in steam for 10 hours at 450°C of films deposited below 450°C by SiH_4 oxidation decreased the film thickness by 8% from the as deposited value.[3]

In a previous project at Caltech[4] we had studied the stability of SiO_2 membranes prepared at 450°C by SiH_4 oxidation in the opposing reactants geometry. This oxidation was carried out both under dry conditions and in the presence of water vapor. Subsequent dry annealing of the membranes reduced slowly the H_2 and N_2 permeances. Annealing in a H_2O-N_2 atmosphere reduced more sharply the H_2 permeance. But the N_2 permeance increased or decreased depending on whether the deposition had been carried out in the absence of presence of water.

In this project the preparation of silica membranes was carried out at temperatures above 600°C and under substantial partial pressures of water vapor. However, the deposition reaction lasted only a few minutes to one hour. It was important, therefore, to examine the stability of the membranes under extended exposure to a gas with a composition similar to that anticipated in a membrane reactor for the water gas shift reaction. For this purpose a number of stability tests were carried out as described below. The first two series of these tests were conducted with a simulated coal gas (including H_2S). The remaining two series of tests were conducted with H_2O-N_2 mixtures, since other than H_2O none of the components of the coal gas was expected to have a significant effect on the annealing process.

The stability testing conducted as part of this project did not examine the effect of trace contaminants in the coal gas. Among these contaminants alkali metal vapors can have a long term deleterious effect by gradually dissolving in the glass structure and reducing the permeance.[5] The content of alkali vapor in the feed to the membrane

reactor would depend on the particular coal and on the preceding particulate removal scheme. A guard bed of silica, silica-alumina, etc. particles could be used to reduce further, if necessary, the alkali content of the gas before introduction in the membrane reactor.

2.2 Apparatus and Procedure

The apparatus for the stability tests consists of a flanged stainless steel cylinder, 1 m long, 3.8 cm ID, connected to a Bourdon pressure gauge and to lines for introduction of various gases and for evacuation. Up to eight membrane tubes could be secured in this cylinder for an extended stability test. After the membrane tubes were placed and secured in the cylinder, an amount of liquid water placed in a crucible was introduced, calculated to produce the desired partial pressure of water at the test temperature. The cylinder was then sealed, evacuated and pressurized with the other gases, one at a time, while recording the pressure increase for each gas. The pressure increase for each gas was chosen to provide the desired partial pressure at the test temperature. After all the gases were introduced, the cylinder was slowly heated by an electrical furnace to the desired test temperature (550 or 600°C) and kept at that temperature for a period from one day to two weeks. At the completion of the heating period, the cylinder was slowly cooled to room temperature and opened. Each membrane tube was then tested for permeance to hydrogen and nitrogen at different temperatures. In some cases the membrane tubes were reintroduced into the pressure cylinder and the procedure of heating, cooling and testing were repeated.

2.3 Results

First Series of Stability Tests

In the first series of stability tests seven tubes were placed in the pressure cylinder and exposed to a gas of composition 22% H_2, 27% CO, 18% CO_2, 32% H_2O, 1% H_2S at 12 atm total pressure and 600°C temperature for two days. Table 2.1 shows the

permeation coefficients before and after the stability test. The results of the stability testing are summarized in Table 2.1 in terms of the H_2 and N_2 permeation coefficients before and after the treatment. With the exception of tube 4 containing B_2O_3 all tubes suffered significant loss of hydrogen permeance, in most cases by a factor of 5-20. Tube No. 5 underwent only a modest loss of hydrogen permeance. This tube had been prepared by SiH_4 oxidation rather than $SiCl_4$ hydrolysis. Most tubes underwent an increase in nitrogen permeance, such that the H_2:N_2 ratio declined, in some cases dramatically. Of all tubes tested only tubes 1 and 5 retained satisfactory hydrogen permeance coefficient as well as satisfactory H_2:N_2 permeance ratio. Tube No. 4 containing the B_2O_3 layer underwent an increase of hydrogen permeance and a larger increase of nitrogen permeance. The final ratio is close to the Knudsen value of 3.74 showing that the B_2O_3 layer lost its integrity during the thermal treatment.

Second Series of Stability Tests

Another series of tests was carried out with several SiO_2 and TiO_2 membranes that had been prepared previously under various conditions. The conditions of membrane preparation and the results of the stability tests are summarized in Tables 2.2-2.4 Table 2.2 lists the stability tests for six SiO_2 membranes, one prepared in the one-sided geometry by $SiCl_4$ hydrolysis, four prepared in the opposing reactants geometry by $SiCl_4$ hydrolysis, and one prepared in the opposing reactants geometry by SiH_4 oxidation. All membranes were subjected to several days of heating at 500 or 600°C, under 10-12 atmospheres total pressure in a gas with 22% H_2, 27% CO, 32% H_2O, 18% CO_2 and 1% H_2S simulating the coal gas from oxygen-blown gasification of a high sulfur coal. In all cases the treatment resulted in a decrease of the H_2 permeance and an increase of the N_2 permeance. All membranes prepared by $SiCl_4$ hydrolysis in the opposing reactants geometry underwent drastic decline of permeance after the first two days of treatment and failed after an additional two-day period. The membrane prepared by $SiCl_4$ hydrolysis in the one-sided geometry and the one prepared by SiH_4 oxidation in the opposing reactants

geometry underwent significant decrease of the H_2 permeance during the first two-day period but little further decrease during the second two-day period. The hydrogen permeance of 0.04-0.06 at 600°C is lower by a factor 3-5 than the permeance measured immediately after deposition. The H_2:N_2 permeance ratios also declined from about 1000 to about 170-280.

Examination of the results of Table 2.2 shows that all membranes prepared by $SiCl_4$ hydrolysis in the opposing reactants geometry failed, while the membrane prepared by the same reaction in the one-sided geometry survived the stability test. To test the stability of membranes prepared in the one-sided geometry further, a fresh membrane was prepared and tested under the conditions summarized in Table 2.3. It should be noted that the deposition of this new membrane was carried out with a larger partial pressure of H_2O compared with membrane No. 5 of Table 2.2 (5% vs. 2.5%). After deposition the membrane was exposed to a total of 7.5 days of hydrothermal treatment. Permeation measurements were carried out immediately after deposition, after 1.5 days of treatment, after 3 days of treatment, and after 7.5 days of treatment. The H_2 permeance at 600°C declined by a factor of four after the first 3 days of treatment and showed no further decline in 4.5 additional days. The final value of 0.075 at 600°C or 0.048 at 450°C appears to be close to the stable value of the fully densified membrane. The H_2:N_2 permeance ratio likewise declined from about 1000 to a final stable value of 750. The results of this long-term stability test can be considered as satisfactory although the final permeance was low.

Similar stability tests were conducted for three TiO_2 membranes prepared by $TiCl_4$ hydrolysis in the opposing reactants geometry. It will be recalled that TiO_2 membranes can be prepared only in the opposing reactants geometry. The conditions of membrane preparation and the results of the stability tests are summarized in Table 2.4. All three tubes underwent significant decline of H_2 permeance after the first two days of

treatment, but little further change after three additional days of treatment. The final stable permeance at 600°C was 0.04-0.07 cm^3/cm^2-min-atm, only a little lower than for the SiO_2 membranes prepared in the opposing reactants geometry (Table 2.3). The H_2:N_2 permeance ratios declined from about 300 to 70-120, substantially below those listed in Table 2.4 for the SiO_2 membranes.

Third Series of Stability Tests

A new series of tests was conducted on a fresh batch of SiO_2 membranes prepared in one-sided and opposing reactants geometries at different temperatures and reactant concentrations in order to test the effect of deposition conditions on membrane stability. In this series several membranes were placed in the high pressure system in contact with a gas containing 30-32% H_2O in nitrogen at 10 atmospheres total pressure and 550°C temperature. The permeation rates of H_2 and N_2 were measured at 450 and 600°C for the membranes as deposited, after 12 hours annealing in dry nitrogen at 750°C, and after exposure to the aforementioned hydrothermal environment for several days as detailed in Tables 2.5-2.7 below.

Table 2.5 shows the results of the stability tests for three membranes deposited in the opposing reactants geometry. After two days of hydrothermal treatment, the permeance of all three membranes declined by a factor of ten to a very low value of 0.003-0.005 cm^3/cm^2-min-atm. No further tests were conducted with these membranes.

The permeance of five membranes prepared by one-sided deposition under different conditions is listed in Table 2.6. After 9 days of hydrothermal treatment (550°C under 3 atm of water vapor), all membranes underwent significant decline of permeance, but membranes 16, 17, 18, and 20 reached respectable hydrogen permeances of about 0.07-0.12 cm^3/cm^2-min-atm. Two of these membranes (16 and 18) were later damaged in handling. The remaining two membranes 17 and 20 were subjected to 12 additional days of drothermal treatment. As detailed in Table 2.7, membrane 17 underwent some

decline of permeance, but membrane 20 showed no further decline of permeance after this additional treatment.

Fourth Series of Stability Tests

A fourth series of tests was conducted with silica membranes coded 24-30 prepared by one-sided deposition as defined in Table 1.2 of the preceding chapter. It will be recalled that this batch of membranes was prepared using two different types of support tubes and three different silica reagents. The permeances of these membranes immediately after deposition, after twelve hours of thermal treatment at 700-750°C, and after thirteen days of additional hydrothermal treatment at 550°C under 3 atm of water vapor are listed in Table 2.8. All membranes prepared in this series underwent hydrothermal treatment with the expected decrease of hydrogen permeance, but no catastrophic change occurred as with the membranes of the first series. Using the dimer and trimer silica precursors gave only a slight improvement in hydrogen permeance and had no consistent effect on H_2:N_2 selectivity. Using the 25 Å pore tubes improved moderately the hydrogen permeance but seemingly reduced the selectivity from about 500-1000 to about 200-300. The best permeance was obtained with membrane 29 made with 25 Å pore size tubes using the dimer precursor. This tube had hydrogen permeance of 0.13 cm^3/cm^2-min-atm with H_2:N_2 selectivity of 200 at 500°C, after the thirteen-day hydrothermal treatment. As stated earlier, the measurement of the very small nitrogen permeance is subject to considerable error from small leaks in the system. Hence the true N_2 permeances may be considerably lower than the measurements indicate, and the calculated selectivities probably significantly underestimate the true selectivities. Activation energies for hydrogen permeance varied somewhat from membrane to membrane but were generally in the range 25-30 kJ/mol with the exception of membrane 25 which gave 39 kJ/mol.

Figure 2.1 shows a sharp increase in the activation energy following deposition and hydrothermal treatment. The permeance of the untreated tube has negative activation

energy in accordance with Knudsen diffusion (permeance inversely proportional to $T^{1/2}$). After deposition and annealing, the activation energy increases to a value about 10 kJ. This value is the result of the series combination of the deposit layer resistance and the resistance of the uncoated tube. After the hydrothermal treatment, the resistance is dominated by the deposit layer, whence the much higher activation energy (~30 kJ/mol).

In addition to the stability tests listed in Table 2.8, a membrane from a previous series (No. 20 of Table 2.6) which had undergone 9 days hydrothermal treatment was subjected to additional 13 days of the same treatment (550°C, 3 atm of water vapor) resulting in only 8% decrease of its hydrogen permeance and no change of selectivity.

Discussion

The results of the preceding series of hydrothermal testing suggest that membrane stability is quite sensitive to the preparation conditions. Membranes produced by $SiCl_4$ hydrolysis in the opposing reactants geometry in most cases cracked during extended hydrothermal treatment. Membranes prepared in the one-sided geometry with $SiCl_4$ partial pressure above 0.1 atm also often cracked upon cooling and reheating. The most stable membranes were those prepared with low partial pressures of $SiCl_4$ (below 0.1 atm) at 700-750°C deposition temperature. These membranes withstood as long as three weeks of heating (550°C with 3 atm H_2O vapor, 7 atm N_2) including one or two intermediate cooling and reheating periods. These membranes also turned out generally to have higher hydrogen permeance than the other membranes. SEM results discussed in the previous chapter show that one-sided SiO_2 deposition with high $SiCl_4$ partial pressures causes homogeneous formation of particles which accumulate on the cylindrical surface outside of the pores of the support tube. The external SiO_2 layer formed under these conditions seems to cause catastrophic thermal expansion/contraction stresses during cooling and reheating. At low $SiCl_4$ concentrations the homogeneous generation of particles is slower and the formation of an external layer limited, with the deposit layer

being confined mainly within the pores of the support. Such thin internal layers evidently do not cause cracking of the support tube upon cooling and reheating.

Literature Cited

1. Swaroop, B., in "Thin Film Dielectrics," Vratny (Ed.), The Electrochemical Soc., New York (1969).
2. Pliskin, W. A., *J. Vac. Sci. Technol.* **14**, 1064 (1977).
3. Kern, W., *RCA Review* **37**, 55 (1976).
4. Nam, S. W. and Gavalas, G. R., *AIChE Symp. Ser.* **85**, 68 (1989).
5. Shelby, J. E., "Molecular Solubility and Diffusion" in *Treatise on Materials Science and Technology*, M. Tomozawa and R. H. Doremus (Eds.), Vol. 17, Academic Press, 1979.

Table 2.1. Permeation coefficients of H_2 and N_2 at 450°C before and after two-day treatment at 600°C with a mixture of 22% H_2, 27% CO, 18% CO_2, 32% H_2O, 1% H_2S at 12 atm total pressure.

	Permeation Coefficients (cm^3/cm^2-min-atm)					
	H_2		$N_2 \times 10^4$		H_2:N_2 ratio	
Membrane Code[a]	Before	After	Before	After	Before	After
15	0.21	0.04	0.28	0.55	7500	727
6	0.07	0.004	0.75	0.1	930	400
7	0.07	0.003	0.42	3.4	1670	9
B1	0.02	0.19	0.24	500	833	3.8
b	0.11	0.07	0.70	3.3	1570	212
8	0.12	0.01	3.0	1.6	400	62
9	0.05	0.005	0.78	3.5	640	14

[a] Membrane codes defined in Tables 1.2 and 1.3 of Chapter 1.

[b] This membrane prepared by silane oxidation (5% SiH_4-N_2; 15% O_2-4% H_2O-N_2).

Table 2.2. Permeation coefficients of SiO_2 membranes after hydrothermal treatment. Treatment I: 2 days at 600°C, 12 atmospheres total pressure, gas composition 22% H_2, 27% CO, 32% H_2O, 18% CO_2, 1% H_2S. Treatment II: 2 days at 500°C, 10 atmospheres total pressure, same gas composition.

		Deposition Conditions			Permeation Coefficients at 600°C (cm^3/cm^2-min-atm)					
					Initial		After Treatment I		After Treatments I + II	
Membrane Code	Geometry	Temperature (°C)	Reactants (%)[a] $SiCl_4$	H_2O	H_2	N_2	H_2	N_2	H_2	N_2
5	one sided	600[b]	2	2.5	0.21	$28x10^{-5}$	0.040	$5.5x10^{-5}$	0.039	$14x10^{-5}$
6	opposing	800	10	8	0.07	7.5	0.004	10	-	-
7	opposing	800	19	8	0.07	4.2	0.003	34	-	-
8	opposing	800	30	8	0.12	30	0.010	16	-	-
9	opposing	800	30	8	0.05	7.8	0.005	35	-	-
c	opposing	450	c	c	0.11	7.0	0.070	33	0.06	35

[a] For opposing reactants composition is given for each reactant stream individually ($SiCl_4$-N_2, H_2O-N_2); for one-sided deposition composition refers to the mixed stream $SiCl_4$-H_2O-N_2.

[b] Annealed at 800°C after the deposition.

[c] Deposition by SiH_4 oxidation using 5% SiH_4, 15% O_2, 4% H_2O.

Table 2.3. Permeation coefficients of a SiO_2 membrane after hydrothermal treatment. The membrane was prepared in the one-sided geometry at 600°C with 2% $SiCl_4$ and 5% H_2O.

Treatment	Permeation Coefficients at 600°C (cm^3/cm^2-min-atm) H_2	N_2
None	0.310	$3x10^{-4}$
I	0.083	2
I + II	0.075	1
I + II + III	0.075 (0.048[a])	1 (0.4[a])

I 1.5 day at 550°C, 10 atm total pressure, gas composition 23% H_2, 27% CO, 32% H_2O, 18% CO_2.

II 1.5 additional days under same conditions as I.

III 4.5 additonal days under same conditions as I.

[a]Permeation coefficients at 450°C.

Table 2.4. Permeation coefficients at 600°C of TiO_2 membranes after hydrothermal treatment.

Membrane No.[b]	Deposition Conditions[a] Temperature (°C)	Time (min)	Reactants (%) $TiCl_4$	H_2O	Permeation Coefficients at 600°C (cm^3/cm^2-min-atm) Initial H_2	Initial N_2	After Treatment I H_2	After Treatment I N_2	After Treatment I + II H_2	After Treatment I + II N_2
T6	600	45	10	20	0.194	7.3×10^{-4}	0.081	8.6×10^{-4}	0.076	8.6×10^{-4}
T7	450	45	10	20	0.145	5.4	0.045	5.2	0.037	5.5
T8	200	35	10	20	0.174	5.7	0.068	6.7	0.067	5.6

Treatment I: 2 days at 550°C, 10 atm total pressure, gas composition: 23% H_2, 27% CO, 32% H_2O, 18% CO_2.

Treatment II: 3 additional days under the same conditions.

[a] All tubes prepared in the opposing reactants geometry.

[b] Codes are defined in Table 1.3 of the previous chapter.

Table 2.5. Permeation coefficients of SiO_2 membranes prepared by opposing reactants deposition after consecutive hydrothermal treatments.

Membrane Code[a]	Permeation Coefficients at 650°C (or 450°C) (cm^3/cm^2-min-atm)							
	Initial		After Treatment I		After Treatment I+II		After Treatment I+II+III	
	H_2	N_2	H_2	N_2	H_2	N_2	H_2	N_2
10	$6x10^{-2}$	$8x10^{-4}$	NA	NA	$3x10^{-3}$	$3x10^{-5}$	NA	NA
6	7	0.7	NA	NA	4	1	NA	NA
9	5	0.7	NA	NA	5	3.5	NA	NA

Treatment I: 12 hours annealing in dry N_2 at 750°C.

Treatment II: 2 days at 550°C, 10 atm total pressure with 32% H_2O-N_2.

Treatment III: 7 days under same conditions as II.

[a] Membrane codes defined in Table 1.2 of Chapter 1.

Table 2.6. Permeation coefficients at 600°C of SiO_2 membranes prepared by one-sided deposition after consecutive hydrothermal treatments.

Membrane Code[a]	Permeation Coefficients at 600°C (or 450°C) (cm^3/cm^2-min-atm)							
	Initial		After Treatment I		After Treatment I+II		After Treatment I+II+III	
	H_2	N_2	H_2	N_2	H_2	N_2	H_2	N_2
16	0.31	0.012	0.37 (0.26)	20×10^{-4} (5)	0.18 (0.082)	10×10^{-4} (4)	0.10 (0.04)	8×10^{-4} (2)
17	0.41	0.004	0.36 (0.22)	10 (2)	0.15 (0.06)	2 (0.7)	0.07 (0.02)	2 (7)
18	0.40	0.0075	0.37 (0.23)	30 (7)	0.14 (0.056)	9.2 (5)	0.075 (0.022)	5 (4)
19	0.40	0.011	0.40 (0.27)	20 (6)	0.17 (0.076)	6 (2)	NA	NA
20	NA	NA	0.33 (0.25)	7 (5)	0.25 (0.11)	6 (5)	0.12 (0.05)	1 (0.5)

Treatment I: 12 hours annealing in dry N_2 at 750°C.

Treatment II: 2 days at 550°C, 10 atm total pressure with 32% H_2O-N_2.

Treatment III: 7 days under same conditions as II.

[a] Membrane codes defined in Table 1.2 of Chapter 1.

Table 2.7. Permeation coefficients of SiO_2 membranes No. 17 and No. 20 of Table 2.6 after additional hydrothermal treatment.

Treatment	Permeation Coefficients at 600°C (450°C) cm^3/cm^2-min-atm			
	Membrane No. 17		Membrane No. 20	
	H_2	N_2	H_2	N_2
I	0.36 (0.22)	$10x10^{-4}$ (2)	0.33 (0.25)	$7x10^{-4}$ (5)
I+II+III	0.07 (0.02)	2 (7)	0.12 (0.05)	1 (0.5)
I+II+III+IV	0.04 (0.015)	8 (1)	0.13 (0.043)	2 (5)

Treatments I, II, and III defined in Table 2.

Treatment IV: 12 days at 550°C, 10 atm total pressure with 30% H_2O-N_2.

Table 2.8. Membrane permeance to hydrogen and nitrogen under various treatments (Treatment II: 12 hours under N_2 at 700-750°C; Treatment II: 13 days at 550°C under 3 atm of water and 7 atm N_2).

		Membrane Permeance (cm^3(STP)/cm^2-min-atm)							
				Immediately After Deposition					
Membrane[a]	Temperature of Measurement (°C)[b]	Before Deposition H_2	Before Deposition N_2	H_2	$N_2 \times 10^3$	After Treatment I H_2	After Treatment I $N_2 \times 10^3$	After Treatment I&II H_2	After Treatment I&II $N_2 \times 10^3$
24	450	0.41	0.11			0.22	0.86	0.06 (404)	0.18 (404)
	600	0.37	0.10			0.25	0.96	0.11	0.21
	750	0.35	0.094			0.27	1.00	0.15 (684)[b]	0.23 (684)
27	450	0.41	0.11			0.21	0.4	0.06 (400)	0.14 (400)
	600	0.37	0.10			0.21	0.3	0.13	0.16
	700	0.35	0.095			0.26	0.3	0.17	0.16
28	700	0.471	0.126	0.322	5.6	0.299	0.22		
30	415							0.06	0.17
	591							0.15	0.3
	700	0.57	0.154	0.465	1.3	0.447	0.55	0.20 (684)	0.51(684)
25	450	1.05	0.31			0.26	3	0.03 (420)	0.4 (420)
	600	0.98	0.29			0.34	2	0.11 (596)	0.7 (596)
	700	0.91	0.27			0.40 (750)	1.6	0.16 (684)	0.8 (684)
29	450	1.05	0.31			0.52	1.3	0.08 (408)	0.8 (408)
	600	0.98	0.29			0.59	1.3	0.20 (592)	0.9 (592)
	700	0.91	0.27			0.63	1.8	0.27 (684)	1.0 (684)

[a] Membrane codes defined in Table 1.2 of Chapter 1.

[b] Certain permeances were measured at different temperatures given in parentheses.

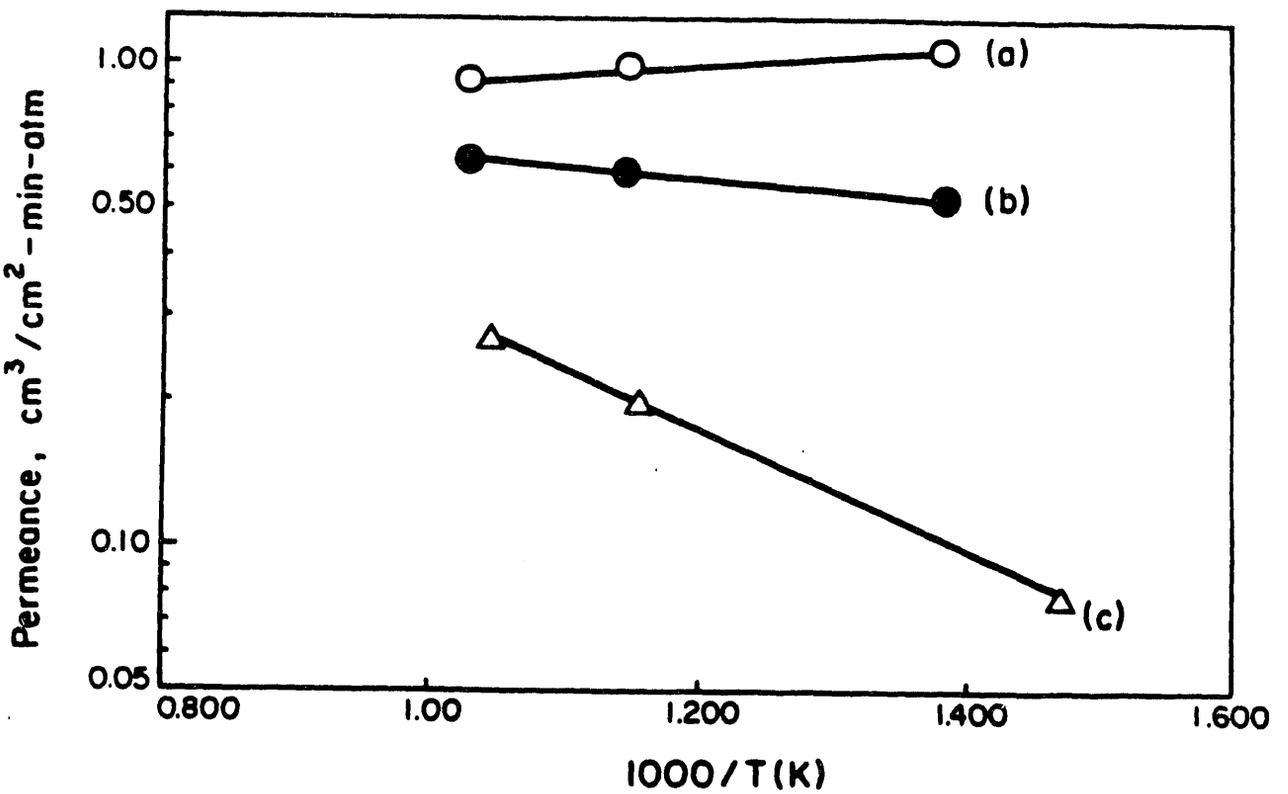

Figure 2.1. Arrhenius diagram of the hydrogen permeance of SiO_2 membrane (a) before deposition, (b) after deposition, and (c) after 13 days at 550°C, 3 atm H_2O.

Chapter 3

Analysis and Economic Evaluation of SiO_2 Membrane Application to Hydrogen Production from Coal Gas

3.1 Introduction

This chapter contains the report of Kinetics Technology International (KTI) (A Mannesmann Company) on work performed under subcontract to this contract. KTI made an economic evaluation of the silica membranes prepared at Caltech for the case of an ammonia-from-coal process. This process was chosen to take advantage of the capability of the silica membranes to produce high purity hydrogen as required for ammonia synthesis. The process analysis and economic evaluation conducted by KTI was based on information on membrane properties and on the operation of the conventional and membrane shift reactors generated at Caltech. An appendix to this chapter describes a membrane shift reactor model developed at Caltech for this purpose.

The KTI study was performed by Mrssrs. R. R. Jungerhans, Manager of Technology Development and Pietro Brandani, Process Engineer. Mr. William Campbell of M. W. Kellog provided information on the composition of coal gas produced by a KRW gasifier and made useful suggestions about power cogeneration associated with the process under consideration.

3.2 Description of the Membrane Shift Reactor

The membrane shift reactor is shown schematically in Figure 3.1. It consists of three fixed bed sulfur resistant shift reactors R-1, R-2, R-3, three membrane units M-1, M-2, M-3, and two heat exchangers, H-1 and H-2 for generation of medium pressure steam. The reactors, membrane units and heat exchangers are interconnected for feed, permeate and non-permeate gas streams as shown. One typical membrane module is schematically shown in Figure 3.2. A membrane module consists of a steel casing containing the capillaries. The bottom end of each capillary is plugged, while the upper end is connected to the plenum through a glass plate. The shell space of each membrane module is kept at a pressure of 20 to 30 atm in order to provide sufficient H_2 partial pressure driving force for hydrogen permeation across the membra Hydrogen

permeate at about 2 atm pressure flows out of the plenum of each module to common hydrogen lines. Details of the membrane module of this study are given below.

Sizing and Capital Cost Estimates of Membrane Units

For the purpose of this study, the membrane capillaries are specified to have 0.5 mm ID, 0.7 mm OD, with a deposited SiO_2 layer near the outside surface. The apparent Vycor glass density is 1.5 gr/cm^3. One square meter of outside membrane area has a capillary length:

$1/pi \times 0.7 \times (10)^{-3} = 454.5$ m/m^2

and a mass: $pi/4 \times (0.7 \times 0.7 - 0.5 \times 0.5) \times (10)^{-2} \times 4550 \times 1.5 = 128.6$ gr

or 0.1286 kg/m^2.

The cost of the capillaries of that size has been very roughly estimated by Corning to be 300 to 600 USD/lb. We shall use 500 USD/lb for our evaluation, corresponding to:

$$0.1286 \times 2.2046 \times 500 = 142 \text{ USD/m}^2$$

The required membrane area has been estimated by Dr. Gavalas for two scenarios as follows:

Scenario 1 is based on a hydrogen permeance of 0.1 cm^3(STP)/cm^2-min-atm, which is the permeance at a baseline operating temperature of 500°C measured for the membranes prepared until recently in Dr. Gavalas' laboratory. This permeance is the stabilized value after hydrothermal treatment.

Scenario 2 is based upon a permeance of 0.3 cm^3(STP)/cm^2-min-atm at 500°C. There are good reasons to expect that the permeance can be increased from 0.1 to 0.3 by certain modifications of the membrane deposition process. Such modifications are currently under investigation at Dr. Gavalas' laboratory.

Membrane Area Requirements and Cost Estimate Per Scenario 1

The total permeate hydrogen is 4635 lbmol/hr or 35000 gmol/min and the estimated split of this flow between the three membrane units is as indicated below:

Membrane unit M-1

hydrogen permeate flow = 14029 gmol/min
average H_2 delta p = 6.5 atm
average T = 551°C
average permeance = 0.1414 cm^3(STP)/cm^2-min-atm
area = 14029 x 22400 x $(10)^{-4}$ / 6.5 x 0.1414 = 3.42 x $(10)^4$ m^2

Membrane unit M-2

hydrogen permeate flow = 11188 gmol/min
average H_2 delta p = 4.65 atm
average T = 543°C
average permeance = 0.1266 cm^3(STP)/cm^2-min-atm
area = 1188 x 22400 x $(10)^{-4}$ / 4.65 x 0.1266 = 4.26 x $(10)^4$ m2

Membrane unit M-3

hydrogen permeate flow = 9855 gmol/min
average H_2 delta p = 2.76 atm
average T = 513°C
average permeance = 0.1097 cm^3(STP)/cm^2-min-atm
area = 9855 x 22400 x $(10)^{-4}$ / 2.76 x 0.1097 = 7.29 x $(10)^4$ m^2

Total membrane area = (3.24 + 4.26 + 7.29) x $(10)^4$ = 15 x $(10)^4$ m^2

Capillaries at 142 USD/m^2: 21.2 MM USD

Estimated Cost of Membrane Modules

One membrane module could be made as a cylinder with 12 cm diameter, 30 cm total length containing 14700 capillaries of 25 cm length, occupying 50% of the module cross section, for a total of 3673 m capillary length or 8.08 m^2 membrane area.

The cost of each module at mass production is estimated at about 100 USD. The total number of modules required is:

15 x $(10)^4$ / 8.08 = 18600 at a total cost of about 1.9 MM USD

The cost of piping, valves and housing is estimated an additional 0.5 MM USD.

The Total Cost of the Membrane Units is: 21.2 + 1.9 + 0.5 = 23.6 MM USD

The membrane modules are divided into the three membrane units M-1, M-2 and M-3 with approximate individual volumes of 25, 31 and 54 m^3, each containing respectively about 4200, 5200 and 9100 modules. The modules are combined in series and parallel. For example, 50 or 100 modules are connected in series in a sub unit and the required number of sub units are connected in parallel to form the unit.

Cost Estimate per Scenario II

Using the higher permeance of 0.3 cm^3(STP)/cm^2-min-atm at 500°C, instead of 0.1 as used in Scenario I and maintaining all other assumptions of Scenario I above, we obtain a total cost for the three membrane units of 23.6 / 3 = 7.9 MM USD.

3.3 Basis of the Study

In this study two hydrogen production processes are compared as follows:

1. A conventional process with a high and low temperature sulfur resistant shift reactor with intercooling, followed by PSA purification.

2. A process utilizing a membrane shift reactor, as described above, followed by methanation.

The feedgas is produced in a KRW oxygen blown gasifier for 1000 mt/d low sulfur (0.4%) Western (Utah) coal. It passes via ash and slag removal and enters the hydrogen production plants free of particulates.

In both processes, hydrogen is produced in an amount equivalent to 560 mt/d ammonia. The balance of the gas is used for generation of power in a gas turbine cogeneration cycle. This power is used for driving the combustion air compressor and the ammonia syngas compressor. All excess steam is converted into power and the power in excess of the needs of the schemes under consideration is exported.

Both processes do not yield purified CO_2 as required for production of urea.

The sulfur content in the gasification gas is about 0.13%. In the non-permeate gas from the membrane shift reactor, it is about 0.19%. It is assumed that these gases can be burned in the gas turbine without further clean-up.

3.4 Process Description

Coal gasification delivers the following feedgas as reported by Kellogg: (see reference page 75).

CO	38.63	vol%
H_2	28.87	
CO_2	10.69	
CH_4	4.99	
N_2	0.70	
Ar	0.70	
O_2	0.00	
NH_3	0.38	
H_2S	0.11	
COS	0.02	
H_2O	14.99	
HCN	95 ppm	
MeOH	0.00	
SUM	**100.00**	

Total flow: 10041 lbmol/hr

Pressure: 412 psig
Temperature: 1925°F

Membrane Shift Process

CO contained in the coal gasification gas is shifted towards CO_2 while producing more hydrogen, and high purity hydrogen is separated in the membrane shift reactor. The permeate gas is the hydrogen rich gas stream. It contains about 1000 ppm CO + CO_2, 130 ppm inerts (CH_4 + N_2 + Ar) and maximum 3 ppm sulfur. This sulfur level is acceptable for the next processing steps of methanation and ammonia synthesis. The permeate gas pressure at 15 psig is relatively low. Therefore, more syngas compression is needed than in the conventional process.

The non-permeate gas at a pressure of 376 psig is used as fuel in a gas turbine for power generation. Because of its high CO_2 content, the heating value of this gas is relatively low (LHV = 163 BTU/SCF), more over, it contains all the sulfur of the coal gasification gas. For the purpose of this study, the assumption is made that no further clean-up of this gas is necessary. The efficiency of the gas turbine after air compression is assumed to be about 25.4%.

The gas composition change and subsequent products split in the membrane shift reactor, as determined by Caltech is given as follows:

Table 3.1 Composition of feed, permeate, and non-permeate (retentate) streams in membrane shift reactor.

	Feed	Non-Permeate	Permeate
CO vol%	33.59	19.46	454 ppm
H_2O	26.08	6.91	283 ppm
H_2	25.10	11.48	99.86
CO_2	9.30	52.22	527 ppm
CH_4	4.34	7.26	99 ppm
$H_2S + COS$	0.11	0.19	3 ppm
$N_2 + Ar$	1.22	2.04	28 ppm
$NH_3 + HCN$	0.27	0.45	6 ppm
	100.00	100.00	100.00

The exothermal reaction heat to be removed at a temperature level high enough for medium pressure steam generation is 0.811 MJ/100 gmol raw gas or 35 MMBTU/hr.

Heat is recovered from the hydrogen containing gas and subsequently the gas is compressed in four stages to about 400 psig. Remaining CO and CO_2 are methanated, the gas is dried and high purity nitrogen from the air separation plant is added to obtain an ammonia syngas with H_2/N_2 ratio of 3:1 and a total inert content of 0.04%. The

ammonia synthesis loop operates at a pressure of about 1500 psig and the ammonia production is approximately 570 MT/d.

In order to prevent inert build-up in the synthesis loop, a small stream is continuously purged from the loop and is added to the fuel for the gas turbine.

All non-permeate gas is burned in the gas turbine for the production of power. The small purge gas flow from the synthesis loop also goes to fuel.

Heat for the generation and superheat of 1250 and 470 psig high and medium pressure steam is recovered from the hot coal gasification gas, the membrane shift reactor, the main process stream and the gas turbine exhaust. The stack temperature is about 400°F. All high pressure steam is run through a back pressure turbine for additional power generation. About 15% of the MP steam at the HP Turbine exhaust is injected into the main process stream to enhance the shift reaction. The remainder of the MP steam is run through a condensing turbine at 5 inch Hg for more power generation. Low temperature heat is recovered for BFW preheat.

A schematic block flow diagram is included at the end of this chapter.

Conventional Process

Starting with the same coal gasification gas as the membrane shift process, about 70% of it is sent to high and low temperature shift conversion. The hydrogen containing gas from the LTS is purified in a PSA, which produces 99.99 plus high purity hydrogen at a recovery of about 92%. Conventional purification with acid gas removal and methanation would result in an ammonia synthesis gas with about 6% methane. With such high inerts content in the synthesis gas, the hydrogen loss via the loop purge would be 2 to 3 times as high as the PSA purge losses, which makes conventional purification impractical. The drawback of PSA purification is the recompression of its purge gas for usage as gas turbine fuel.

Hydrogen product for both processes is about equal and equivalent to an ammonia production of 560 MT/d. The coal gasification gas contains about 0.15% H_2S. The high

and low temperature shift catalysts are, therefore, sulfur resistant as for example BASF's K 8-11. H_2S and CO_2 are removed in a PSA. High purity nitrogen from an air separation plant is added to obtain an ammonia synthesis gas with H_2/N_2 ratio of 3:1. The pressure at the syngas compressor inlet is about 370 psig, which is considerably higher than the permeate gas pressure of the membrane shift process. The syngas compression is accordingly lower.

The purge gas from the synthesis loop is small and theoretically approaches zero.

The remaining 30% of the coal gasification gas is used as fuel in a gas turbine for power generation. The sulfur content of the fuel gas is the same as in the coal gasification gas (0.13%). The heating value is about 160 BTU/SCF, which is comparable to the membrane shift process. Again, this gas is used in the gas turbine, without further treatment. The turbine efficiency, after combustion air compression is again assumed about 25.4%. The purge gas from the synthesis loop is added to fuel in the gas turbine.

The steam generation and heat recovery is similar as in the membrane shift process as follows: 1250 and 470 psig high and medium pressure steam are generated in the hot coal gasification gas, the process gas leaving the shift reactors and using the gas turbine exhaust. The stack temperature is about 400°F. All high pressure steam is run through a back pressure turbine for additional power generation. The total high pressure steam generation is about 80 MT/hr, which is about the same as for the membrane shift process. In order to obtain a 99+% CO conversion in the shift reactors, about 75% of the medium pressure steam of the high pressure turbine exhaust is injected into the main process stream. This is about five times the quantity needed in the membrane shift process. The remainder of the medium pressure steam is run through a condensing turbine at 5" Hg for more power generation. Low temperature heat is recovered for BFW preheat.

A schematic block flow diagram is included at the end of this chapter.

3.5 Comparison of Processes

Both processes have been evaluated on the same basis with the same efficiencies for the gas turbine, the steam turbines, similar stack temperature, etc. The ammonia synloop for both processes is practically identical, and in this report, is not considered as a contributing factor to the capital and/or operating cost difference between the two processes.

In terms of overall efficiency, the processes compare as follows:

Table 3.2 Comparison of operating characteristics of the membrane-assisted and conventional process.

		Membrane	Conventional
Feedgas	lbmol/hr	10041	10041
NH_3	Mt/d	560	555
Export power	MW	44.4	36.6
or in	MM BTU/hr (LHV)		
Feedgas	@250 Btu/SCF	953	953
NH_3	@8000 Btu/lb	419	415
Export power	@3412 Btu/kWhr	151	125
Efficiency %		60	57

Starting with the same gasification gas the battery limits products of both processes are as follows:

		Membrane	Conventional
Ammonia product	MT/d	560	555
Export power	MW	44.4	36.6

The power production for both processes is itemized as follows:

		Membrane	Conventional
Gas turbine output	KW	86640	78860
Combustion air compressor		55400	47300
		31240	31560
HP turbine		5870	5515
MP turbine		19025	11320
		55780	48750
Syngas compressor		10430	4130
Purge gas compressor		0	7070
		45350	37550
Pumps, fans		980	920
Netto export		44370	36630

Note the following differences between the operations:

The net output of the gas turbine, after combustion air compression and the HP steam turbine outputs are about the same. The membrane process takes much less MP pressure steam and therefore, the MP steam turbine output for the membrane process is larger than for the conventional process.

As the pressure of the purified hydrogen for the membrane process is lower than in the conventional process, the syngas compressor power for the membrane process is larger than for the conventional process. These two effects are counteracting and the resulting power balance at this point is about equal.

In the conventional process, the PSA purge gas needs to be recompressed to the 400 psig level, whereas, in the membrane process, the pressure drop of the non-permeate gas in the membrane reactor is small and no recompression is necessary. As smaller power users for both processes are comparable, the nett power export for the membrane

process is about 7.7 MW more than for the conventional process, which is roughly equal to the power of the purge gas compressor of the conventional process.

Depending on the kWhr unit price, the operating cost advantage of the membrane process over the conventional process is:

for 2ct/kWhr : 1.3 MM USD/yr
for 5ct/kWhr : 3.1 MM USD/yr

Capital Costs of Membrane Shift Reactors

Professor Gavalas has developed two scenarios for the cost of the membrane units as follows:

Scenario I	MM USD	23.6
Scenario II		7.9
Difference:		**15.7**

Scenario I is based upon currently available permeances. Senario II is for permeances expected to result from improvements in the deposition process.

With an operating advantage for the membrane between 1 and 3 MM USD/yr, depending on the kWhr unit price, the best simple pay out for the extra cost of Scenario I is between 5 and 15 years, which is too long a period. Scenario I appears to be too costly.

We consider Scenario II for the Membrane Shift process of this study and have the following comparisons with the conventional process:

Equipment of one process, which does not exist in the other:

- Membrane Process:
  - Membrane shift reactor, including membrane units/modules shift reactors, and heat exchangers
  - Methanator
  - Dryer
  - MP turbine (larger capacity)
- Conventional Process:
  - HTS
  - LTS
  - Exchangers HX-1, HX-11
  - PSA

The cost of the larger syngas compressor of the membrane process is about equal to the cost of the smaller syngas compressor of the conventional process plus its purge gas compressor.

The overriding importance for the economics of the membrane process is the cost of the Vycor glass tubes which is quoted to be between 300 and 600 USD/lb. As basis for this study, 500 USD/lb is taken. This is very expensive material. To view this number in perspective, the following unit prices are given for comparison:

Gold	350	USD/ounce or	5000 USD/lb
Silver	4	USD/ounce or	58 USD/lb

In other words, the membrane glass unit price turns out to be the geometric average of silver and gold!

The estimated installed capital difference for the two processes, being Membrane Scenario II vs Conventional, based on the above indicated equipment, is as follows:

Membrane	MM USD	11
Conventional		6
Difference		**5**

For the membrane process, about 80% of its cost is contributed to the membrane units; for the conventional process the PSA is the main contributor.

As stated before, the cost of the membrane units depends heavily on the Vycor glass unit price. The PSA has a capacity of about 40 MM SCF/d of H_2. Its estimated price is fairly accurate.

The estimated capital extra for the membrane process of about 5 MM USD is paid back by the extra power generated in this process, in approximately 1.5 to 4 years, depending on the assumed power unit price.

3.6 Process Optimization

There are opportunities to improve the membrane process by optimizing its operating conditions. For instance, so far the membrane process has been evaluated with a 2 atm abs. permeate pressure. If this pressure is lowered to 1 atm abs. the driving force of the hydrogen through the membrane goes up and the membrane surface and its cost are reduced accordingly. However, the cost of the syngas compression increases.

This particular optimization of the permeate pressure works out as follows for Scenario II:

Membrane unit M-1

average H_2 delta p = 7.5 atm
average permeance = 0.1414 x 3 = 0.4242
area = 14029 x 22400 x $(10)^{-4}$ / 7.5 x 0.4242 = 0.99 x $(10)^4$ m^2

Membrane unit M-2

average H_2 delta p = 5.65 atm
average permeance = 0.1266 x 3 = 0.3798
area = 11188 x 22400 x $(10)^{-4}$ / 5.65 x 0.3798 = 1.17 x $(10)^4$ m^2

Membrane unit M-3

average H_2 delta p = 3.76 atm
average permeance = 0.1097 x 3 = 0.3291
area = 9855 x 22400 x $(10)^{-4}$ / 3.76 x 0.3291 = 1.78 x $(10)^4$ m^2

Total membrane area = (0.99 + 1.17 + 1.78) x $(10)^4$ = 3.9 x $(10)^4$ m^2

Capillaries cost at 142 USD/m^2: 5.6 MM USD

Total cost of membrane units including piping module cost, etc.:

5.6 + 0.5 + 0.1 = 6.2 MM USD

Cost savings over membrane operating at 2 atm abs.: 7.9 - 6.2 = 1.7 MM USD

The increase of the operating costs of the syngas compressor is one extra stage of about 1600 kW. With this modification, the extra capital of the membrane process is 3.3 MUSD, and the extra net power produced is 6 MW. Depending on the price of power, the extra capital investment for the membrane will pay for itself in 1.3 - 3.4 years.

3.7 Summary and Conclusions

In this study we have compared two processes for production of hydrogen.

1. A novel process with a membrane/shift reactor
2. A conventional process with high and low temperature shift conversion plus PSA purification.

Hydrogen product is converted into ammonia at a capacity of 560 MT/d. Unrecovered hydrogen is used for power generation.

The membrane shift reactor employs special glass membrane tubes, whose performance is still being tested at Caltech. For an optimistic performance scenario of the membrane tubes, we have estimated that the extra investment of the membrane process is about 3.3 MM USD more than the investment of the conventional process at the same ammonia production capacity. Excess power of the membrane process is about 6 MW more than of the conventional process. Depending on the assumed power unit price as basis for the evaluation, the extra investment for the membrane process pays for itself in 1.3 to 3.4 years.

The economics of the membrane process will greatly improve when the costs of the Vycor glass tubes come down.

Optimization of the operating conditions of the membrane process will provide opportunities to improve the economics of this novel process.

3.8 Reference

Private communication of W. M. Campbell of M. W. Kellogg Company to G. R. Gavalas: Material balance of the gasifier section of a coal to ammonia plant using KRW oxygen blown gasifier (Coal based KRW case Rev 0, August 3, 1990, stream 7: gasifier product to quench).

R-1
SHIFT REACTOR $9M^3$

M-1
MEMBRANE UNIT
SCENARIO I $25M^3$
SCENARIO II $8.3M^3$

H-1
HEAT EXCHANGER

R-2
SHIFT REACTOR $9M^3$

M-2
MEMBRANE UNIT
SCENARIO I $31M^3$
SCENARIO II $10.3M^3$

H-2
HEAT EXCHANGER

R-3
SHIFT REACTOR $9M^3$

M-3
MEMBRANE UNIT
SCENARIO I $54M^3$
SCENARIO II $18M^3$

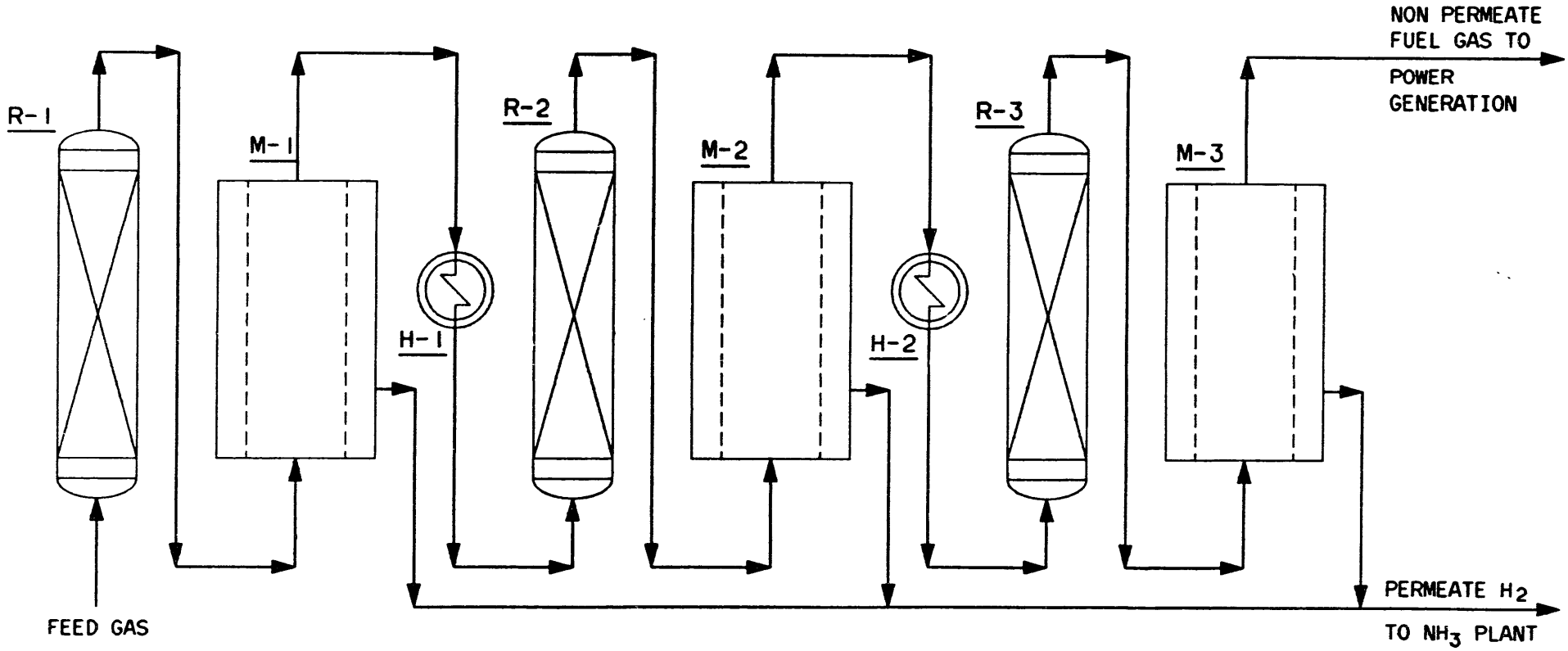

NOTE:
EACH MEMBRANE UNIT CONTAINS 20-200 PARALLEL SUB-UNITS, EACH SUB-UNIT CONSISTS OF ABOUT 50 MEMBRANE MODULES IN SERIES.

MEMBRANE SHIFT REACTOR

FIG. 3.1

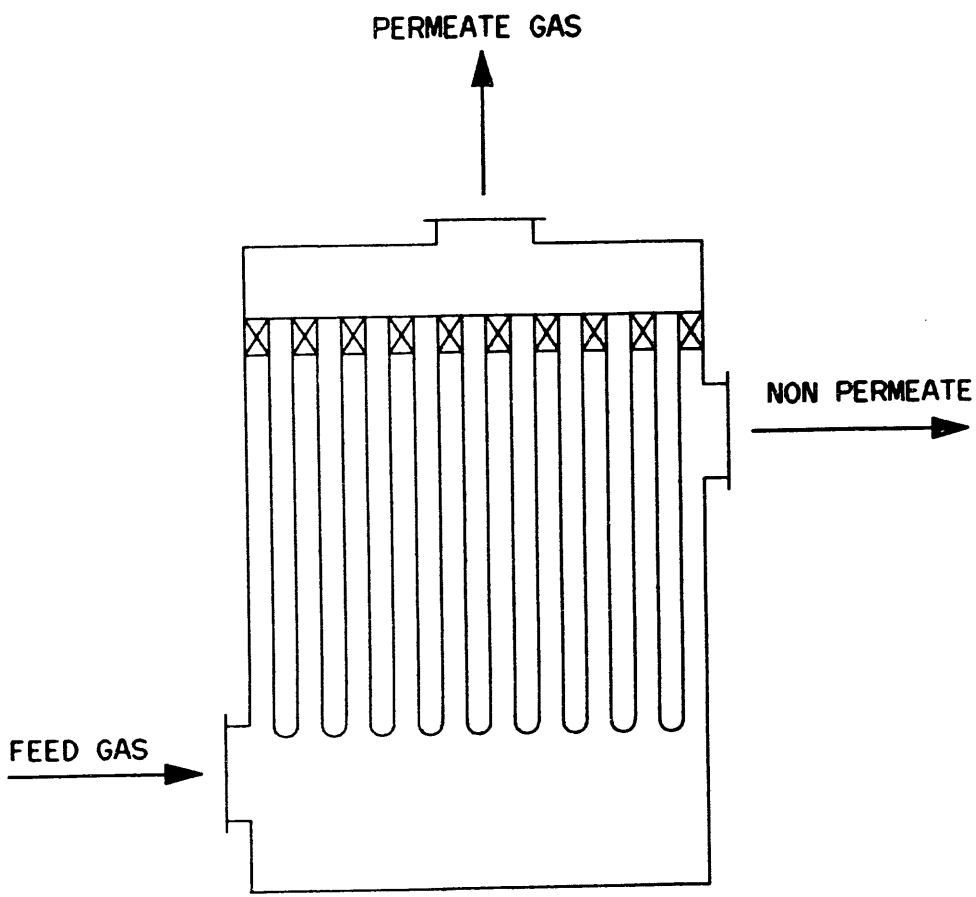

MEMBRANE MODULE
CIRCULAR CROSS SECTION ABOUT 12 CM DIA.
CONTAINING ABOUT 14700 CAPILLARIES 0.5 MM I.D.,
0.7 MM O.D. AND 25 CM IN LENGTH.

MEMBRANE MODULE

FIG. 3.2

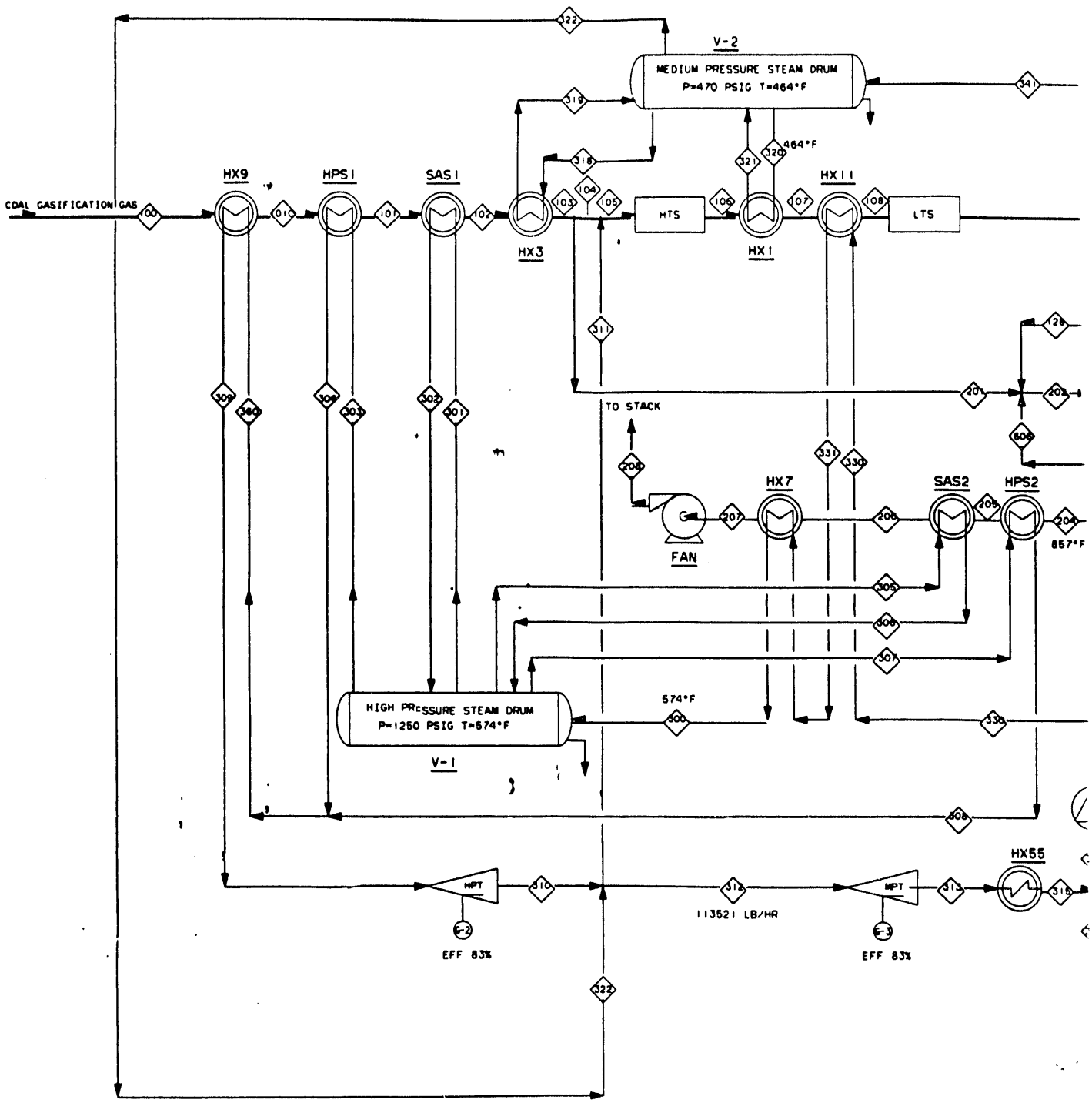
V-2
MEDIUM PRESSURE STEAM DRUM
P=470 PSIG T=464°F
464°F
HX9
HPS1
SAS1
HX3
HTS
HX1
HX11
LTS
COAL GASIFICATION GAS
TO STACK
HX7
SAS2
HPS2
857°F
FAN
HIGH PRESSURE STEAM DRUM
P=1250 PSIG T=574°F
V-1
574°F
HX55
MPT
MPT
G-2
G-3
EFF 83%
EFF 83%
113521 LB/HR

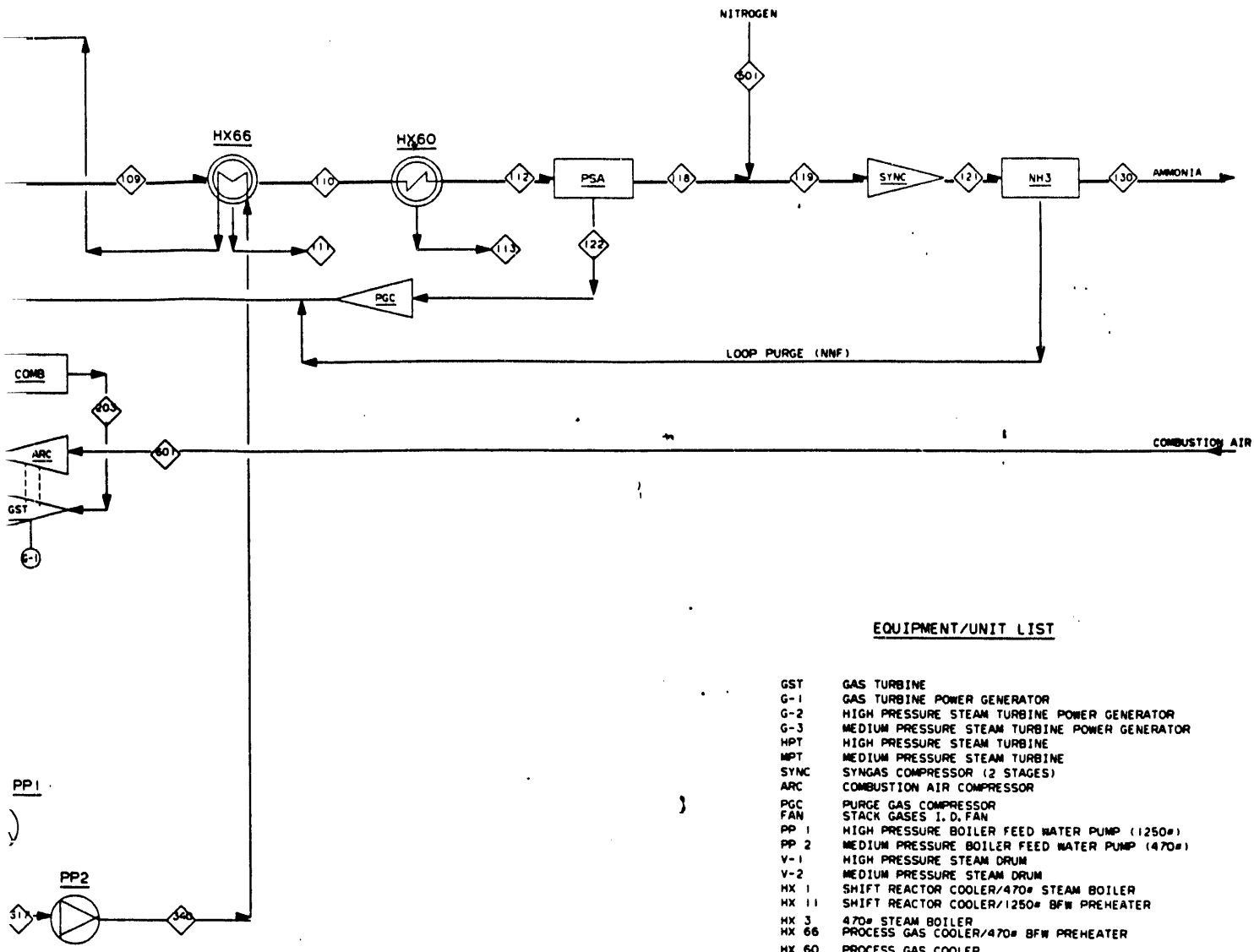

EQUIPMENT/UNIT LIST

GST	GAS TURBINE
G-1	GAS TURBINE POWER GENERATOR
G-2	HIGH PRESSURE STEAM TURBINE POWER GENERATOR
G-3	MEDIUM PRESSURE STEAM TURBINE POWER GENERATOR
HPT	HIGH PRESSURE STEAM TURBINE
MPT	MEDIUM PRESSURE STEAM TURBINE
SYNC	SYNGAS COMPRESSOR (2 STAGES)
ARC	COMBUSTION AIR COMPRESSOR
PGC	PURGE GAS COMPRESSOR
FAN	STACK GASES I. D. FAN
PP 1	HIGH PRESSURE BOILER FEED WATER PUMP (1250#)
PP 2	MEDIUM PRESSURE BOILER FEED WATER PUMP (470#)
V-1	HIGH PRESSURE STEAM DRUM
V-2	MEDIUM PRESSURE STEAM DRUM
HX 1	SHIFT REACTOR COOLER/470# STEAM BOILER
HX 11	SHIFT REACTOR COOLER/1250# BFW PREHEATER
HX 3	470# STEAM BOILER
HX 66	PROCESS GAS COOLER/470# BFW PREHEATER
HX 60	PROCESS GAS COOLER
HPS 2	1250# STEAM SUPERHEATER
SAS 2	1250# STEAM BOILER
HPS 1	1250# STEAM SUPERHEATER
SAS 1	1250# STEAM BOILER
HX 9	1250# STEAM SUPERHEATER
HX 55	CONDENSER
HX 7	ECONOMIZER
HTS	HIGH TEMPERATURE SHIFT
LTS	LOW TEMPERATURE SHIFT
PSA	PRESSURE SWING ABSORBER
COMB	GAS TURBINE COMBUSTION CHAMBER
NH3	AMMONIA SYNTHESIS LOOP

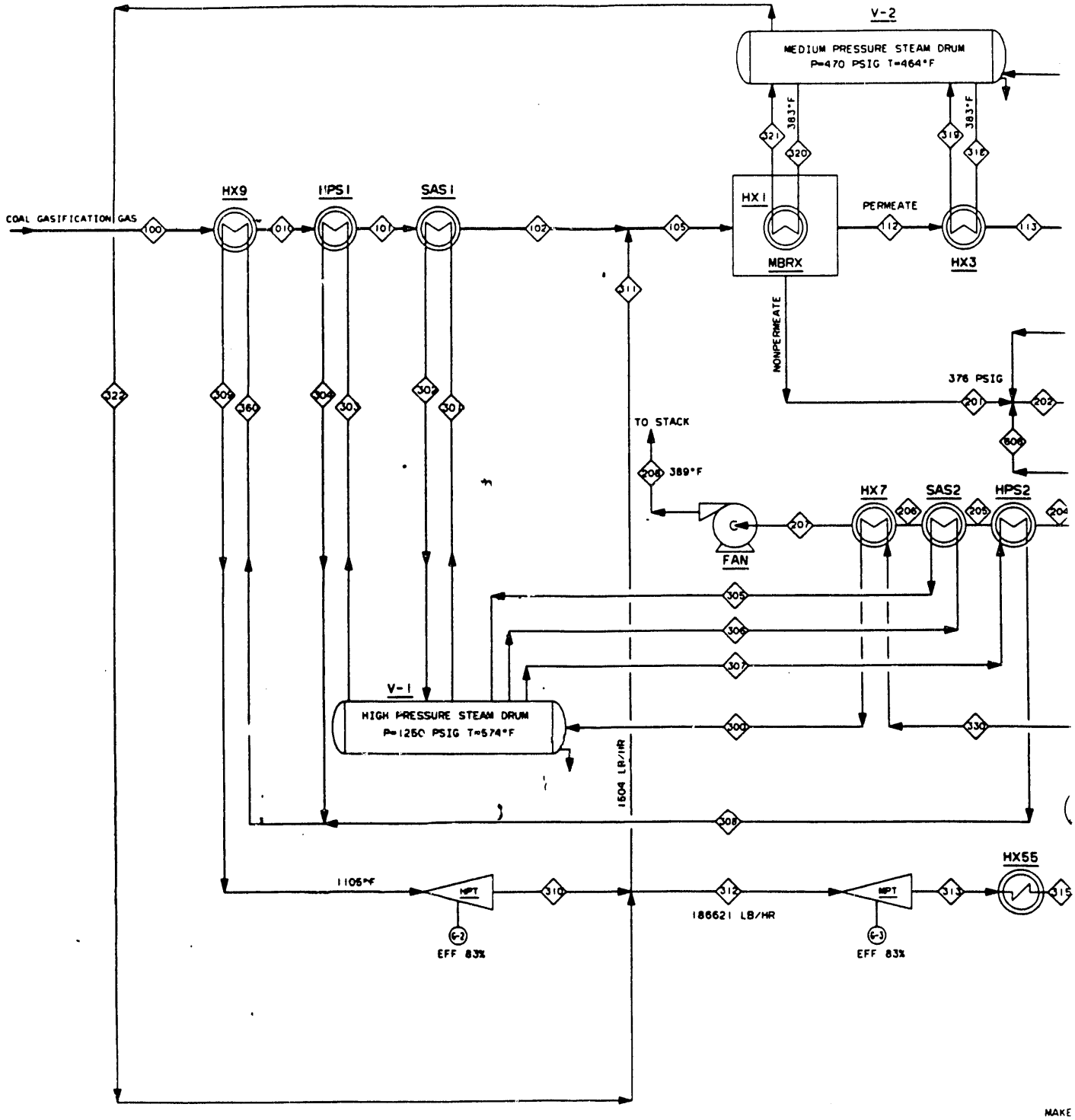
V-2
MEDIUM PRESSURE STEAM DRUM
P=470 PSIG T=464°F
383°F
383°F
321
320
319
318
HX9
IIPS1
SAS1
HX1
MBRX
PERMEATE
HX3
COAL GASIFICATION GAS
100
101
102
105
112
113
111
NONPERMEATE
376 PSIG
201
202
203
322
309
304
307
TO STACK
208
389°F
HX7
SAS2
HPS2
FAN
207
206
205
204
305
306
307
V-1
HIGH PRESSURE STEAM DRUM
P=1250 PSIG T=574°F
300
330
1604 LB/HR
308
HX55
1105°F
MPT
310
312
186621 LB/HR
MPT
313
315
6-2
EFF 83%
6-3
EFF 83%
MAKE

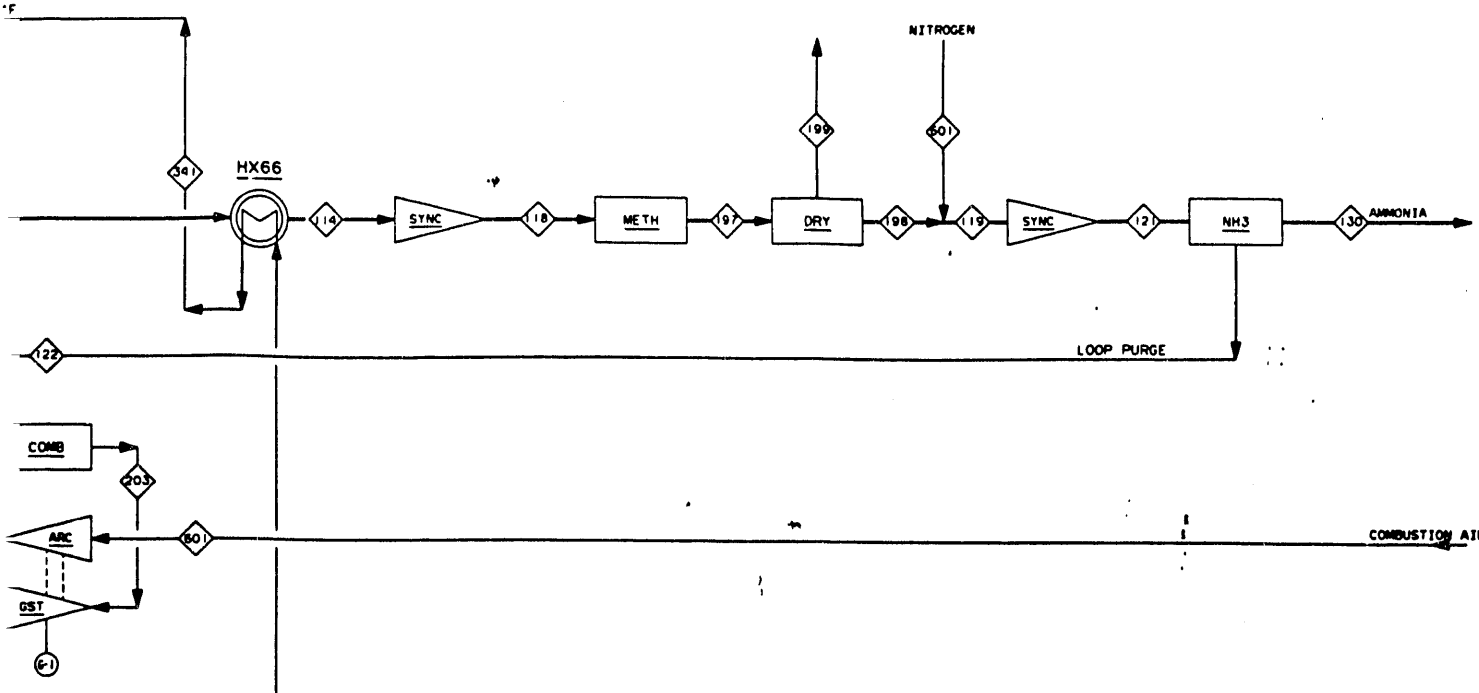

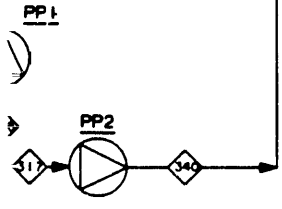

WATER

EQUIPMENT/UNIT LIST

GST	GAS TURBINE
G-1	GAS TURBINE POWER GENERATOR
G-2	HIGH PRESSURE STEAM TURBINE POWER GENERATOR
G-3	MEDIUM PRESSURE STEAM TURBINE POWER GENERATOR
HPT	HIGH PRESSURE STEAM TURBINE
MPT	MEDIUM PRESSURE STEAM TURBINE
SYNC	SYNGAS COMPRESSOR (6 STAGES)
ARC	COMBUSTION AIR COMPRESSOR
FAN	STACK GASES I.D. FAN
PP 1	HIGH PRESSURE BOILER FEED WATER PUMP (1250#)
PP 2	MEDIUM PRESSURE BOILER FEED WATER PUMP (470#)
V-1	HIGH PRESSURE STEAM DRUM
V-2	MEDIUM PRESSURE STEAM DRUM
HX 1	REACTOR COOLER/470# STEAM BOILER
HX 3	470# STEAM BOILER
HX 66	PROCESS GAS COOLER/470# BFW PREHEATER
HPS 2	1250# STEAM SUPERHEATER
SAS 2	1250# STEAM BOILER
HPS 1	1250# STEAM SUPERHEATER
SAS 1	1250# STEAM BOILER
HX 9	1250# STEAM SUPERHEATER
HX 55	CONDENSER
HX 7	ECONOMIZER
MBRX	MEMBRANE SHIFT REACTOR/SEPARATOR
METH	METHANATOR REACTOR
COMB	GAS TURBINE COMBUSTION CHAMBER
DRY	DRYER UNIT
NH3	AMMONIA SYNTHESIS LOOP

DISTRIBUTION (Kilfen)

E F G

Appendix

Model of the Membrane Shift Reactor

APPENDIX. MODEL OF THE MEMBRANE SHIFT REACTOR

1. General Features of Membrane Reactor Design

The membrane reactor is shown schematically in Figure 1a. It consists of one or more batteries of membrane modules connected in series and enclosed in a steel casing (the figure shows one such battery of modules). Cooling elements operating either by ordinary heat exchange or by injection of liquid water may be placed at one or more locations along the battery. The coal gas feed enters at elevated pressure into the leftmost module, flows through the series of modules and exits the last module at the right. Hydrogen permeate at about 1 atm pressure flows out of each module to a common hydrogen line.

A typical module is shown schematically in Figure 1b. It consists of a steel casing containing a large number of membrane capillaries about 200 μm OD, 150 μm ID and 20 cm length. The bottom end of each capillary is plugged, while the upper end is connected to the plenum through a glass plate. The catalyst is packed in pellet form within special modules (not containing membrane capillaries) employed in series with the membrane modules, one catalyst module every five to ten membrane modules. Alternatively (not shown in the Figure) the catalyst may be deposited on the membrane capillaries directly and thus be continuously distributed along the reactor. Each cooling element is located immediately preceding a catalyst module as shown in the Figure. But the cooling modules will generally be fewer than the catalyst modules. The shell space within each membrane module is held at a pressure of 10-20 atm in order to provide sufficient hydrogen partial pressure driving force for hydrogen permeation across the membrane. The interior of the capillaries and the plenum is held slightly above

atmospheric pressure to drive the flow of hydrogen to the common hydrogen line held at atmospheric pressure.

2. Mathematical Model

In the mathematical model described below, the membrane surface and the catalyst surface are treated as continuously and uniformly distributed along the membrane-reactor battery, rather than as being employed in discrete modules. However, heat transfer is still assumed to occur at discrete locations. Figure 2 shows this continuous mathematical model. The following notation is used in formulating the reactor equations:

A_{sh}	cross sectional area of shell, excluding capillaries (cm^2)
a_c	capillary internal radius (cm)
a_i	coefficient of c_{pi} (dimensionless)
b_i	coefficient of c_{pi} (K^{-1})
c_i	coefficient of c_{pi} (K^{-2})
c_{pi}	specific heat of species i (J/mol-K)
E	activation energy of k (J/mol-K)
E_{mi}	activation energy of k_{mi} (J/mol-K)
f_{ci}	total molar flowrate of species i from capillary interior to plenum (hydrogen line) for a single capillary, function of z (mol/s)
f_c'	molar flowrate is capillary of species 1+2+3+4+5
F_{si}	molar flowrate of species i in shell in z-direction, function of z (mol/s)
F_{ST}	total molar flowrate in shell, function of z (mol/s)
F_{To}	total molar flowrate of feed (mol/s)
h	length step in numerical integration (cm)

K_p	reaction equilibrium constant, function of T (dimensionless)
k	reaction rate constant
k_{mi}	mass transfer coefficient of species i through membrane per unit capillary length (mol/cm-s-atm)
k_{mio}	preexponential factor of k_{mi} (mol/cm-s-atm)
l	capillary length (cm)
N_c	number of capillaries per unit reactor length (cm^{-1})
p_c	pressure in capillaries (atm)
p_s	pressure in the shell (atm)
r	reaction rate per unit length of reactor (mol/cm-s)
R	gas constant (8.314 J/mol-K)
T	temperature, function of z(K)
T_o	initial temperature (K)
T_1	reference temperature (K)
T_{max}	maximum permissible temperature (K)
T_{min}	temperature following a cooling stage (K)
y_{ci}	mol fraction of species i in capillaries, function of z
y_{si}	mol fraction of species i in shell, function of z
y_{sio}	initial mol fraction (in the feed)
Z	reactor length (cm)
β	catalyst volume/shell volume
v_i	stoichiometric coefficient in i in shift reaction
ΔH°	standard heat of the shift reaction, function of temperature

Thermodynamic Relationships

$$c_{pi} = R(a_i + b_i T + c_i T^2) \tag{1}$$

$$\Delta H^\circ(T) = H_1 + R\left(\Delta a T + \frac{\Delta b}{2} T_2 + \frac{\Delta c}{3} T^3\right) \tag{2}$$

where

$$\Delta a = \sum v_i\, a_i \qquad \Delta b = \sum v_i\, b_i, \qquad \Delta_c = \sum v_i\, c_i \tag{3}$$

$$H_1 = \Delta H(T_1) - R\left(\Delta a T_1 + \frac{\Delta b}{2} T_1^2 + \frac{\Delta c}{3} T_1^3\right) \tag{4}$$

$$\ln \frac{K_p(T)}{K(T)} = \frac{H_1}{R}\left(\frac{1}{T_1} - \frac{1}{T}\right) + \Delta a \ln \frac{T}{T_1} + \frac{\Delta b}{2}\left(T - T_1\right) + \frac{\Delta c}{6}\left(T^2 - T_1^2\right) \tag{5}$$

Stoichiometry

$$\underset{1}{CO} + \underset{2}{H_2O} = \underset{3}{H_2} + \underset{4}{CO_2} \tag{6}$$

In addition to the four species labeled 1-4 above, we will label as species 5 all other species not participating in this reaction (N_2, H_2S, etc.). The stoichiometric coefficients are $v_1 = -1$, $v_2 = -1$, $v_3 = 1$, $v_4 = 1$ $v_5 = 0$.

Species Balances

$$\frac{dF_{si}}{dz} = -N_c\, f_{ci} + v_i r \qquad i = 1, \ldots, 5 \tag{7}$$

where the reaction rate r per unit reactor length which is the net of the forward and reverse directions is given by

$$r = \beta A_{sh} k c_{s1} \left(1 - \frac{1}{K_p} \frac{y_{s3}\, y_{s4}}{y_{s1}\, y_{s2}}\right) \tag{8}$$

where c_{s1} is the shell concentration of species 1; i.e. CO. This expression may be rewritten as

$$r = k^* \frac{\exp(-E/RT)}{T} y_{s1} \left(1 - \frac{1}{K_p} \frac{y_{s3}\, y_{s4}}{y_{s1}\, y_{s2}}\right) \tag{9}$$

The capillary flowrates f_{ci} are given by

$$f_{ci} = lk_{mi}\, p_{si} \qquad i = 1,\ 2,\ 4,\ 5 \tag{10}$$

$$f_{c3} = lk_{m3}\left(p_{s3} - y_{c3} p_c\right) \tag{11}$$

Equation (10) incorporates the approximation of $y_{ci} \ll 1$ for $i \neq 3$, based on the high membrane selectivity for hydrogen. To eliminate y_{c3} from (11) we use

$$y_{c3} = \frac{f_{c3}}{f_{c3} + f_c'} \simeq 1 - \frac{f_c'}{f_{c3}} \tag{12}$$

where

$$f_c' = \sum_{j \neq 3} f_{cj} \tag{13}$$

so that

$$f_{c3} = lk_{m3} \left(p_{s3} - p_c\right) \left[1 + \frac{f_c'}{f_{c3}} \frac{p_c}{p_{s3} - p_c}\right] \tag{14}$$

and solving for f_{c3}:

$$f_{c3} = \frac{l\, k_{m3}}{2} \left(p_{s3} - p_c \right) \left[\left(1 + \frac{4 p_c f_c'}{l k_{m3} (p_{s3} - p_c)^2} \right)^{\frac{1}{2}} + 1 \right] \tag{15}$$

The capillary relationship (10)-(15) incorporate the assumption of negligible pressure drop along each capillary. This assumption has been found valid for the parameter values of interest.

The partial pressures in the shell, p_{si}, are given by

$$p_{si} = y_{si}\, p_s = \frac{F_{si} p_s}{F_{ST}} \tag{16}$$

$$F_{ST} = \sum F_{sj} \tag{17}$$

With equations (9), (10), (15)-(17), the right hand side of Eqs. (7) functions of T and F_{si} ($i = 1, \ldots, 5$).

In addition to the basic dependent variables T, F_{si}, we would like to keep track of the cumulative flowrates of the various components in the gas stream removed continuously along the reactor. The cumulative flowrates will be denoted by F_{cci} and are clearly given by

$$F_{cci} = N_c \int_0^z f_{ci}\, dz \qquad i = 1, \ldots, 5 \tag{18}$$

From the computer programming standpoint it is convenient to use these equations in the differential equation form

$$\frac{dF_{cci}}{dz} = N_c\, f_{ci} \tag{19}$$

considered simultaneously with the differential equations for F_{si}. In the numerical calculations below we have only considered the cumulative flowrate of hydrogen

F_{cc3} and the total cumulative flowrate $F_{ccT} = \sum F_{cci}$, so that we can monitor the purity of the hydrogen-rich stream obtained through the membrane capillaries.

Energy Balance

$$\left(\sum F_{si}\, c_{pi}(T)\right) \frac{dT}{dz} = \left|\Delta H^{o}(T)\right| r \tag{20}$$

It can be shown that Eq. (18) applies despite the distributed removal of gases (mainly hydrogen) through the capillaries. The reaction rate r can be expressed as a function of T and F_{si} by virtue of the relations already established.

Initial Conditions

These involve feed total flowrate, composition and temperature:

$$z = 0: \quad F_{ST} = F_{T_o}; \quad y_{si} = y_{sio}; \quad T = T_o \tag{21}$$

Reactor Cooling

The energy balance, Eq. (18), does not include any term for cooling because cooling is best carried out in discrete cooling stages as shown schematically in Figure 1. In the simulations below we have assumed that cooling stages will be incorporated as necessary to prevent the temperature exceeding a certain maximum value imposed by either membrane stability considerations or equilibrium considerations. This constraint is incorporated in the numerical integration of the equations by imposing the condition

$$\text{If} \quad T(z) > T_{max} \quad \text{at some } z \text{ then we set} \tag{22}$$

$$T(z + h) = T_{min} \tag{23}$$

where T_{max} is the maximum permissible temperature, h is the step length in the numerical integration, and T min is chosen as some sufficiently low starting temperature for the next reactor section, but not as low as to quench the reaction. One can optimize the location and load of the cooling stages, but this has not been attempted in the simulations below.

3. Numerical Solution and Sample Results

The mathematical model was formulated as a set of 8 simultaneous ordinary differential equations for $F_{si}(i = 1, \ldots, 5)$, T, F_{ccT}, F_{cc3}. The numerical solution was obtained by 4^{th} order Runge-Kutta method. The following base values were chosen for the various parameters.

$T_1 = 700K$

$K_p\ (T_1) = 9.42$

$$k_{mi} = 5.06x10^{-7}\ \exp\left(-\frac{60,000}{RT}\right)\ \ \frac{mol}{cm-s-atm}\quad i = 1,2,4,5$$

$$k_{m3} = 5.50x10^{-5}\ \exp\left(-\frac{37,000}{RT}\right)\ \ \frac{mol}{cm-s-atm}$$

$$k = 5,814\ \exp\left(-\frac{48,500}{RT}\right)\ \ s^{-1}$$

	a_i	$b_i x10^3$	c_i	y_{sio}
1	3.38	0.557	0	0.25
2	3.47	1.45	0	0.39
3	3.25	0.422	0	0.20
4	5.46	1.04	0	0.15
5	3.93	1.49	0	0.01

N_c = 500 cm^{-1}

a_c = 0.05 cm

ℓ = 20 cm

A_{sh} = 400 cm^2

Z = 100 cm

β = 0.01

p_c = 1 atm

p_s = 20 atm

F_{T_o} = 1 mol/s

h = 1 cm

T_o = 723 K (Figure 3), 773 (Figure 4)

T_{max} = 883 K (Figure 3), 823 (Figure 4)

T_{min} = 773 K (Figure 3 and Figure 4)

Sample Calculations

The parameters for cases 1 and 2 are listed above. The only parameters that differ among cases 1 and 2 are T_o and T_{max} as defined above. Figure 3 shows temperature, conversion and two mole fractions along the reactor calculated for the parameters of case 1. Only one cooling module was required causing a drop of temperature from 875 to 780 K. The mole fraction of CO in the shell declines from its initial value of 0.25 to 0.047 while that of H_2 in the shell goes from 0.2 to 0.053. The mol fraction of hydrogn in the hydrogen product stream is 0.996. There

is less than 0.5% of other gases (CO, H_2O, CO_2) in that stream, which is one of the advantages of the membrane reactor. The conversion can be defined in two way:

$$X_1 = \frac{F_{s}CO(0) - F_{s}CO(Z)}{F_{s}CO(0)}$$

$$X_2 = \frac{F_{CCH_2}(Z)}{F_{s}CO(0) + F_{sH_2}(0)}$$

The first definition is based on CO and is the customary definition for conversion of an ordinary reactor. It neglects the very small amount of CO going through the membrane to the hydrogen stream. The second definition is based on the hydrogen separated in almost pure form as a fraction of the total potential hydrogen in the feed (H_2 + CO). It is a more meaningful measure of the combined reaction- separation performance of the membrane reactor. From the numerical results we obtained X_1 = 0.886, X_2 = 0.865. For the same feed conditions, a conventional shift reactor operating with one cooling stage would yield equilibrium conversion 0.656.

The results of the second case study are shown in Figure 4. Because of the lower T_{max}, this reactor includes for cooling stages yielding conversions X_1 = 0.90, X_2 = 0.860. The results are not too difficult from those of case 1.

To evaluate the performance of the membrane reactor it is necessary to take into account the purity of the hydrogen stream, the possible requirements for removing the H_2S content in that stream, the size of the stream going through acid gas removal, the size of the recycle stream and other factors relative to the corresponding performance of a conventional reactor. These comparisons are within the scope of Task 4, economic analysis to be carried out by KTI corporation.

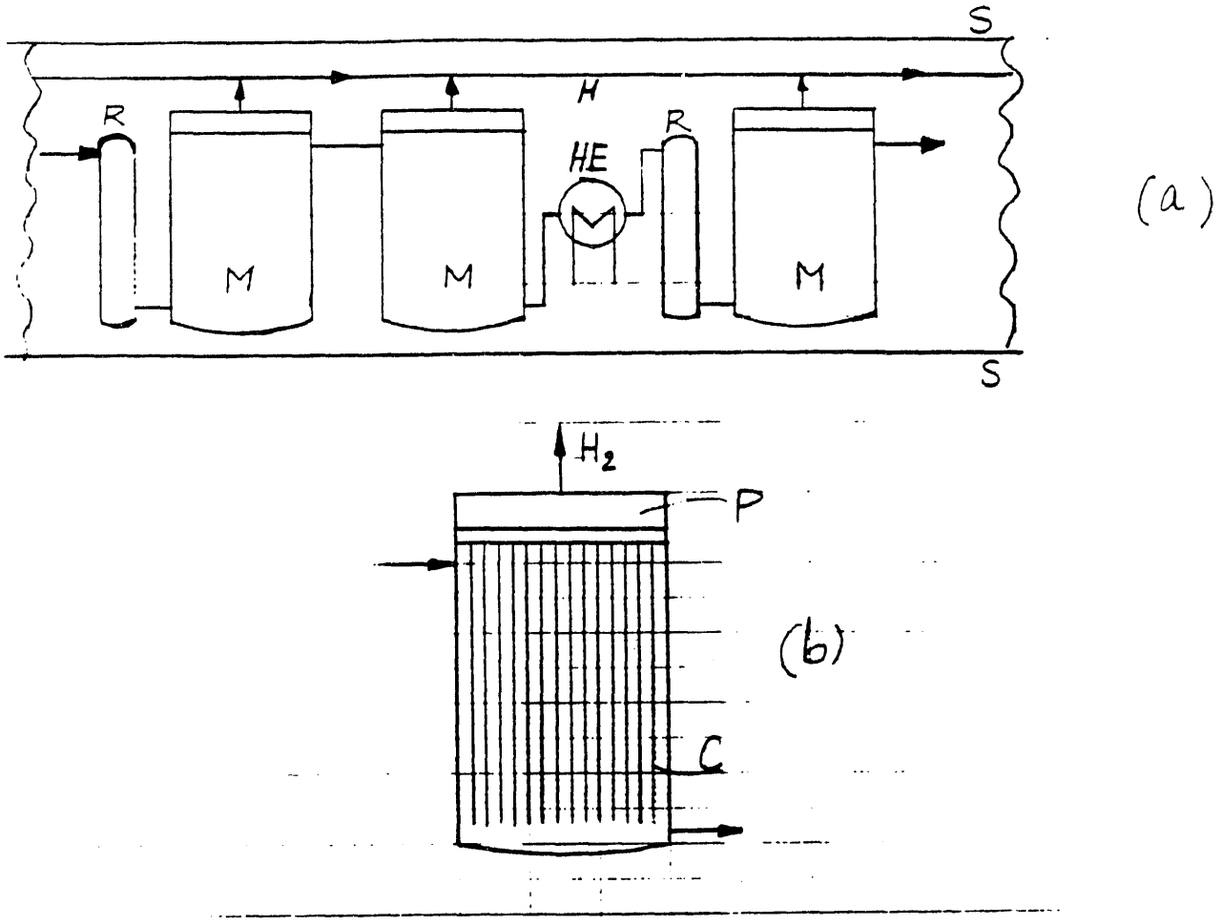

Figure 1. Schematic of a section of a membrane reactor (a) and a membrane module (b). M: membrane module; R: catalyst module; HE: heat exchange module; H: hydrogen line; S: reactor shell; P: plenum; C: membrane capillary.

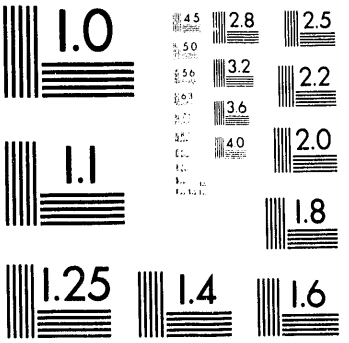
1.0
1.1
1.25
1.4
1.6
1.8
2.0
2.2
2.5
2.8
3.2
3.6
4.0
4.5
5.0
5.6

2 of 2

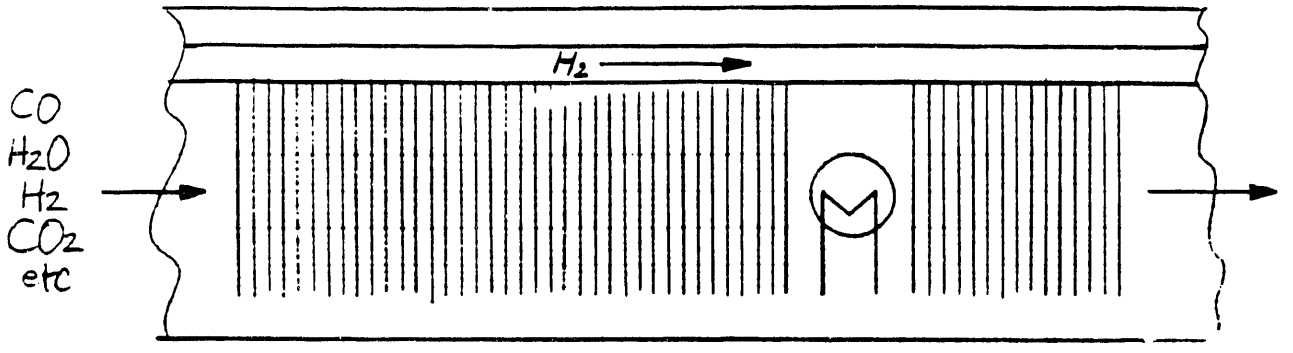

Figure 2. Schematic of the membrane reactor model assuming uniformly distributed catalyst and membrane area, discrete cooling steps.

Figure 3. Temperature, conversion, yH2, yCO along shift reactor.

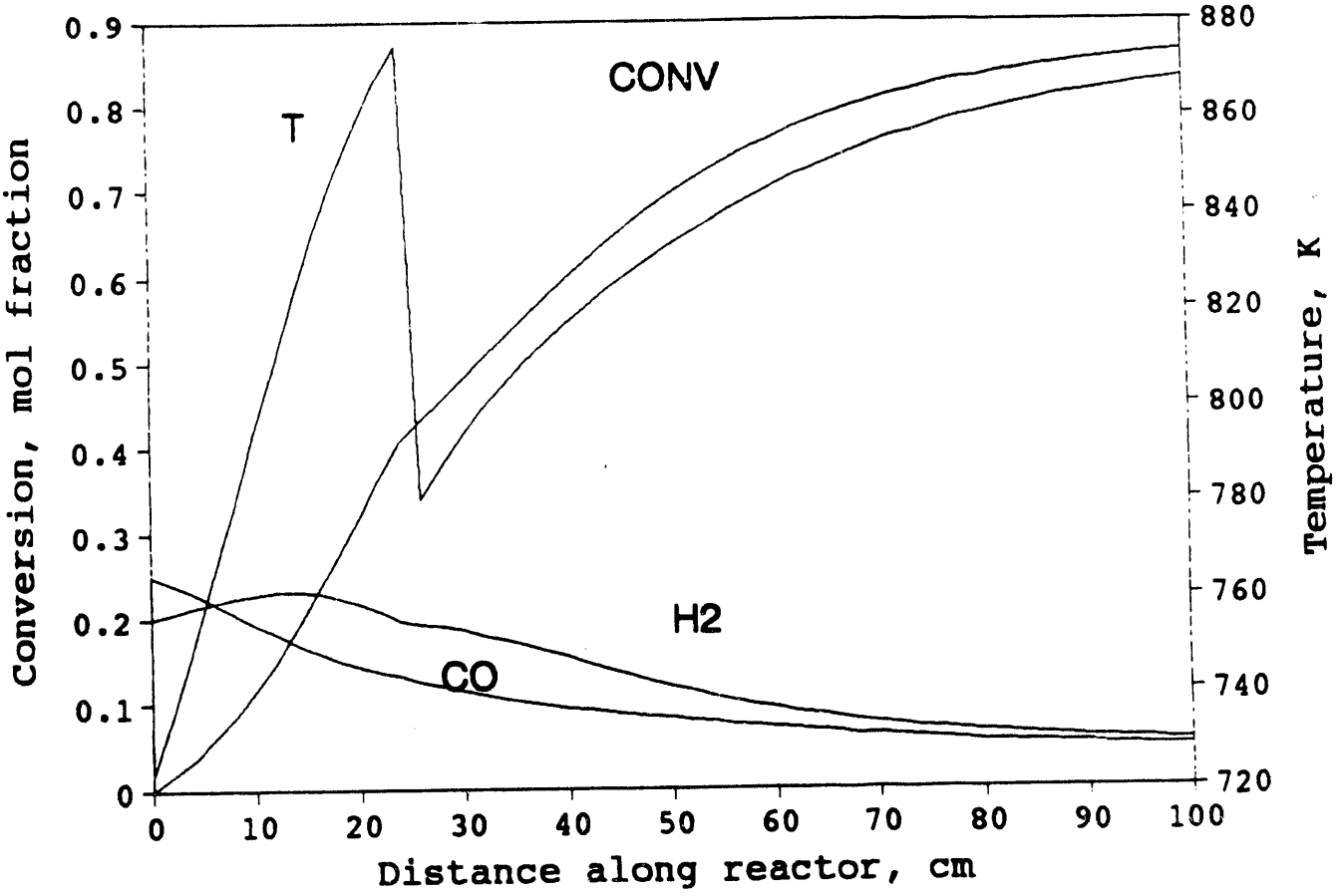

Figure 4. Temperature, conversion, yH2, yCO along shift reactor

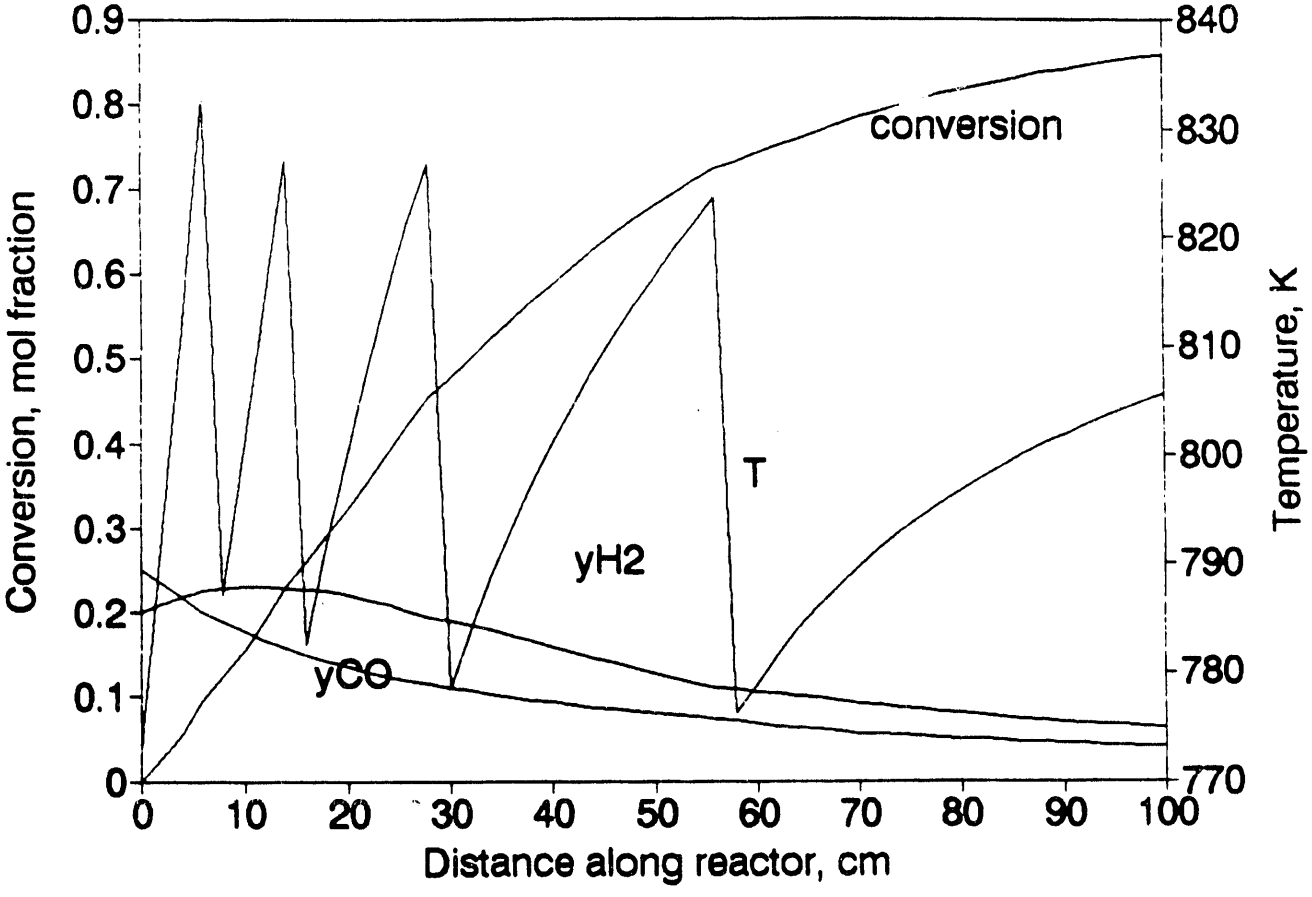

Chapter 4

Conclusions

1. This project has demonstrated the feasibility of preparing membranes highly permselective to hydrogen by CVD of dense SiO_2, TiO_2, Al_2O_3 and B_2O_3 layers within the wall of porous Vycor tubes. The SiO_2 membranes were superior in hydrogen permeance and selectivity, followed by the TiO_2 membranes. The Al_2O_3 membranes had permeance and selectivity considerably below those of the TiO_2 membranes. The B_2O_3 membranes showed some interesting permeation properties but failed upon heating after prolonged exposure to humid laboratory air.

2. Alumina and titania membranes could be prepared only by opposing reactants deposition. Silica and boria membranes could be produced by one-sided deposition as well as by opposing reactants deposition. The silica membranes prepared by one-sided deposition had higher hydrogen permeance but lower selectivity than those prepared by opposing reactants deposition.

3. Annealing of the membranes in dry nitrogen at 700-750°C for 12 hours reduced slightly (0-10%) the permeance of hydrogen and reduced substantially the permeance of nitrogen thus improving the hydrogen selectivity. However, upon extended hydrothermal exposure to 550°C and 3 atmospheres of water vapor for two to three weeks, the hydrogen permeance declined by a factor of 3-5 to a new seemingly stable level. This decline is evidently due to an increase of activation energy for diffusion accompanying the transformation of the highly defective initial deposit layer to a structure similar to that of Vycor glass. The permeance to nitrogen underwent a similar decline such that selectivity was not significantly changed by the hydrothermal treatment. During stability testing the silica membranes were also subjected to twice or three times to cooling and reheating, from 550°C to room temperature and back to 550°C. Membranes prepared by opposing reactants deposition or by one-sided deposition using large pressures of $SiCl_4$ often developed

cracks during these repeated temperature changes. By contrast, membranes prepared by two-sided deposition using $SiCl_4$ pressures below 0.1 atm were stable to repeated cooling and reheating. The most favorable conditions for silica membrane preparation were about 750°C temperature, small $SiCl_4$ pressure (e.g. 0.02 atm) and relatively high H_2O pressure (0.05 atm or higher). The membranes prepared under these conditions had stable hydrogen permeance (after 2-3 weeks of hydrothermal treatment) of about 0.1 $cm^3(STP)/cm^2$-min-atm at 500°C.

4. An evaluation of the commercial potential of the silica membranes was carried out with reference to an ammonia-from-coal process. A conventional and a membrane-assisted process with the same consumption of coal and production of ammonia were compared. The two processes differed only in the amount of electrical power cogenerated. Because of higher efficiency the membrane process had higher net power generation. An economic evaluation of the extra power generated versus the extra capital cost of the membrane process required data on the cost of Vycor tubing and module fabrication. Reliable data are not available at this time because Vycor tubing of the desired dimensions is not commercial and module fabrication has not yet been demonstrated. Only some crude estimates could be made. These estimates suggest that with the currently achievable hydrogen permeance (stabilized value) and with the price of electricity in the range of 2c-5c/kWh the extra cost of the membrane process would be recovered in 5-13 years. This recovery period is too long. If the membrane permeance could be increased by a factor of 3, or the cost of Vycor tubing reduced by the same factor, the extra capital cost of the membrane process would be recovered in only 0.6-1.5 years which would make the process competitive.

5. The experience gained from the membrane preparation experiments and from parallel mathematical modeling studies of the deposition process suggest that the hydrogen permeance can be significantly increased by certain variations of the basic deposition process. The most straightforward of these variations is to use a more reactive silica precursor. Using support tubes with smaller pores and thinner walls, or composite tubes having a thin surface layer of the smaller pores is another possible means of achieving higher permeance. In parallel with a program to increase membrane permeance, it is essential to develop module fabrication techniques. These two efforts can then be followed by longer stability testing at a larger scale than is possible with single membrane tubes. When progress has been made in these two directions it should be possible to obtain more accurate cost estimates for economic evaluation.

DATE
FILMED
11/22/93
END